





ARTICLE

<https://doi.org/10.1038/s41467-019-13320-0>

OPEN

Contribution of oxic methane production to surface methane emission in lakes and its global importance

Marco Günthel^{1*}, Daphne Donis ², Georgiy Kirillin³, Danny Ionescu ⁴, Mina Bizic⁴, Daniel F. McGinnis ^{2*}, Hans-Peter Grossart ^{4,5*} & Kam W. Tang^{1*}

Recent discovery of oxic methane production in sea and lake waters, as well as wetlands, demands re-thinking of the global methane cycle and re-assessment of the contribution of oxic waters to atmospheric methane emission. Here we analysed system-wide sources and sinks of surface-water methane in a temperate lake. Using a mass balance analysis, we show that internal methane production in well-oxygenated surface water is an important source for surface-water methane during the stratified period. Combining our results and literature reports, oxic methane contribution to emission follows a predictive function of littoral sediment area and surface mixed layer volume. The contribution of oxic methane source(s) is predicted to increase with lake size, accounting for the majority (>50%) of surface methane emission for lakes with surface areas >1 km².

¹Department of Biosciences, Swansea University, SA2 8PP Swansea, UK. ²Aquatic Physics Group, Department F.-A. Forel for Environmental and Aquatic Sciences (DEFSE), Faculty of Science, University of Geneva, 1211 Geneva, Switzerland. ³Department of Ecohydrology, Leibniz Institute of Freshwater Ecology and Inland Fisheries, 12587 Berlin, Germany. ⁴Department of Experimental Limnology, Leibniz Institute of Freshwater Ecology and Inland Fisheries, 16775 Stechlin, Germany. ⁵Institute of Biochemistry and Biology, Potsdam University, 14476 Potsdam, Germany. *email: marcoguenthel@gmail.com; daniel.mcginnis@unige.ch; hgrossart@igb-berlin.de; k.w.tang@swansea.ac.uk

After carbon dioxide, methane is the second most important carbon-based greenhouse gas^{1,2}, and its continuous increase in the atmosphere is a global climate threat^{3,4}. A basic premise in methane biogeochemistry is that biological methane formation occurs exclusively under anoxic conditions^{5,6}. Over the past several decades⁷ there have been multiple reports of paradoxical methane oversaturation in oxic sea and lake waters (Tang et al.⁸ and references herein). This methane paradox can be resolved by attributing the methane to conventional anoxic sources^{9,10}, or by additionally considering oxic–water methane production (OMP). The idea of OMP goes against the long-standing paradigm in methane research, and despite the skepticism^{11,12}, different investigators have confirmed repeatedly that methane production can and does occur under oxic conditions in sea and lake waters^{13–16}, and studies have begun to identify the responsible organisms^{17–19} and the underlying biochemical pathways^{17,20}. Unlike anoxic methane sources in sediments and bottom waters, methane production in the surface-mixed layer (SML) places the methane source closer to the water–air interface, and therefore its contribution to surface emission can be significant^{8,21}.

Globally, it is estimated that freshwaters account for (mean \pm minimum error range) $122 \pm 60 \text{ Tg yr}^{-1}$ methane to the atmosphere (ca. 20% of the total emission)²². However, this emission value is not well constrained as indicated by the large uncertainty range²², and leads to disagreement between bottom-up and top-down methane budgets^{22,23}. The large uncertainty of freshwater emission during upscaling is commonly attributed to highly variable methane density fluxes within and across systems^{24–27}, scarcity of long-term data, which do not cover high ecosystem variability^{22,28}, and uncertainties in global freshwater areas^{29–31}. Oxic methane production (OMP) has so far not been considered in global assessments, including methane budgets^{22,23} and IPCC reports^{1,2} despite its potential to contribute significantly to methane density fluxes in freshwater systems^{15,21,32}. For more accurate modeling of freshwater emission and corresponding contribution to the global methane budget, a better understanding of internal methane production, consumption, and distribution pathways is needed.

While methanogenic Archaea are largely responsible for anoxic methane production^{6,33}, primary production has been associated with the oxic methane source^{15,17,32,34}. Therefore, the oxic and anoxic sources will react differently to environmental factors. Global methane budget assessments and future climate change predictions will benefit from proper distinction of oxic versus anoxic methane sources and identifying their individual contribution to the system-wide emission. Bogard et al.³² conducted experiments in Lake Cromwell (Canada) and estimated that OMP accounted for 20% of the total surface emission, with the rest originating from anoxic sources. Likewise, Donis et al.²¹ estimated that OMP was the main methane source in the SML of Lake Hallwil (Switzerland) and accounted for 63–83% of the surface emission (value updated, see Supplementary Note 1 including Supplementary Fig. 1, Supplementary Tables 1 and 2). While both studies demonstrate that OMP can be an important source of methane emission, it is not clear if OMP is a general phenomenon in lakes and what may explain the different contribution patterns in different lakes.

Unlike the open ocean, oxic methane production in lake waters can be confounded by anoxic methane input from the littoral zone. To resolve this, we conducted a study in Lake Stechlin where we used experimental enclosures (Leibniz-Institute of Freshwater Ecology and Inland Fisheries, The Lake Lab; <https://www.lake-lab.de> (2012); Supplementary Fig. 2a) to examine the lake-water methane dynamics without the influence from the littoral zone. Lake Stechlin is a medium-size (4.25 km^2) meso-

oligotrophic lake with a mean depth of 22.7 m (max. 69.5 m) in Northeastern Germany (Supplementary Fig. 2b). It has negligible river in-/outflow, small groundwater-feed³⁵ and has been monitored for decades by the Leibniz Institute for Freshwater Ecology and Inland Fisheries (IGB)³⁶. The Lake Lab installed in Lake Stechlin's South basin consists of a series of experimental enclosures (with periodic water exchange) and a central reservoir (no water exchange since installation in 2011/2012). Methane oversaturation in the lake's surface oxic layer has been observed since 2010^{15,16,34}. Throughout the years 2014, 2016, and 2018 we measured dissolved methane concentration, surface methane emission, and environmental parameters (temperature, dissolved oxygen, algal pigments, and wind speed) in the Northeast and South basins and inside the enclosures (see Supplementary Table 3 for data overview). We then used the data to conduct a detailed methane mass balance analysis for the SML, accounting for the different sources and sinks (Fig. 1), including lateral methane input and OMP under different seasonal conditions (mixed and stratified seasons), and compared our mass balance results to earlier findings. Finally, we combined our findings with literature data to develop a predictive model for oxic methane contribution in relation to lake morphology, and discussed its significance in the global context. Our results show that the contribution of oxic methane source to lake surface emission increases with lake size. Accordingly, in lakes larger than 1 km^2 (or with a littoral sediment area to SML volume ratio smaller than $0.07 \text{ m}^2 \text{ m}^{-3}$) the oxic source dominates methane surface emission. Applying the predictive model to the global lake inventory ($\geq 0.01 \text{ km}^2$) shows that oxic methane production may account for up to 66% of lake methane emission worldwide. This finding highlights that future assessments of global methane emissions should include oxic methane source(s) and that more research is needed to understand the impact of oxic methane production in various lake types and its responses to environmental perturbation such as global warming and widespread eutrophication.

Results

Environmental condition. Temperature and buoyancy frequency N^2 profiles indicate that Lake Stechlin was completely mixed in 2016 until April (Supplementary Fig. 3). At the end of April 2016, the lake started to warm and thermal stratification was established during May. From June to August, the lake was clearly stratified with temperatures $\geq 20^\circ \text{C}$ in the SML. As the stratified water column was mainly sampled during June and July, we refer to this period as the stratified period unless stated otherwise. The thickness of the SML was about 5 m during June, and 6 m in July and August.

Throughout the study period, the water column never turned anoxic, with dissolved oxygen reaching up to ca. 17 mg l^{-1} (ca. 170% saturation) typically 1 m below the methane peak (Supplementary Fig. 4).

Methane concentration. With the onset of stratification, methane concentrations in the oxic upper water column in both Northeast and South basins increased sharply, reaching up to 1400 nmol l^{-1} at thermocline depth (6 m). The SML remained oversaturated with methane throughout the stratified season in both basins ($400\text{--}900 \text{ nmol l}^{-1}$), while methane concentrations were less than 200 nmol l^{-1} at $>10 \text{ m}$ depth (Fig. 2a, b).

Inside the experimental enclosures (water exchanged with open-lake water 2 weeks prior to sampling), methane concentrations were also at over-saturation level in the SML ($300\text{--}400 \text{ nmol l}^{-1}$) with a profile similar to the open water, except for a smaller methane peak at the thermocline (Fig. 2c, d). In contrast, the central reservoir (water never exchanged since installation in 2011/2012) showed a

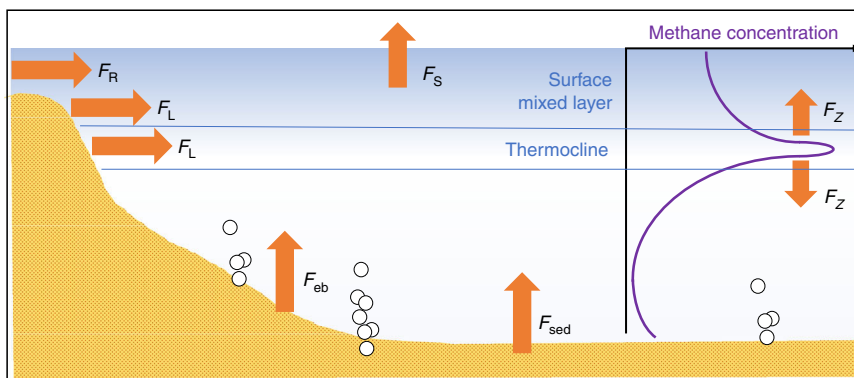


Fig. 1 Methane fluxes in lakes. The typical methane profile of the lake water column has a distinct peak within the thermocline. Methane is introduced into the surface mixed layer horizontally by lateral transport from peripheral water bodies (F_R) and littoral sediments (F_L) and vertically via (turbulent) diffusion (F_Z) originating from bottom sediments (ebullitive flux F_{eb} , diffusive flux F_{sed}). Methane is released to the atmosphere (F_S) across the water-air interface. Biological modulation accounts for additional methane sink and source. Methane loss due to oxidation by methanotrophs is commonly acknowledged, whereas oxic methane production in the surface mixed layer represents an overlooked part of the global methane cycle (e.g., IPCC 2007¹ and IPCC 2013²) (picture drafted as after Donis et al.²¹).

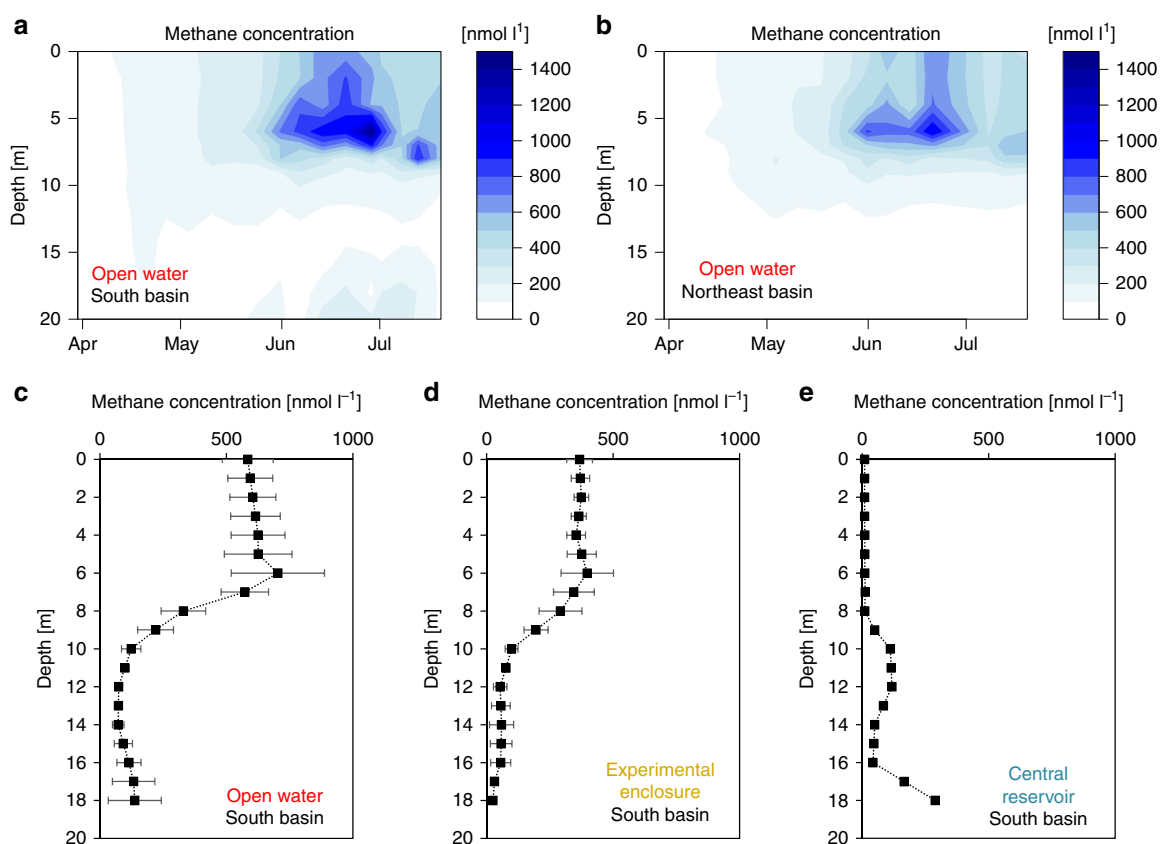


Fig. 2 Methane accumulation in the water column. Panel **a** shows the in situ methane concentration [nmol l^{-1}] recorded weekly in 2016 in the South basin ($53^{\circ}08'36.6''\text{N } 13^{\circ}01'42.8''\text{E}$). Increasing concentration indicates accumulation. Panel **b** shows the methane concentration [nmol l^{-1}] recorded weekly in 2016 in the Northeast basin ($53^{\circ}09'20.2''\text{N } 13^{\circ}01'51.5''\text{E}$). Note, panel **a** contains an additional data point compared to panel **b** in the end of June. Panel **c** shows the methane profile in the open lake of the South basin ($53^{\circ}08'36.6''\text{N } 13^{\circ}01'42.8''\text{E}$; 20.5 m deep) as mean \pm SD of 4 profiles taken on 4 different days in August 2014. Panel **d** shows the methane profile inside experimental enclosure 1 ($53^{\circ}08'36.4''\text{N } 13^{\circ}01'41.6''\text{E}$; ca. 20 m deep) as mean \pm SD of 4 profiles taken on 4 different days in August 2014. Panel **e** illustrates the methane profile inside the central enclosure ($53^{\circ}08'35.8''\text{N } 13^{\circ}01'41.1''\text{E}$; ca. 18.5 m deep) as mean \pm SD of methodological duplicate measurement taken on 7th July 2016. Source data are provided as a Source Data file.

completely different profile during the stratified period, with negligible amount of methane in the SML ($\leq 15 \text{ nmol l}^{-1}$) and higher concentration of methane below 16 m (300 nmol l^{-1}) (Fig. 2e). The small peak (120 nmol l^{-1}) at 12 m depth in the central reservoir methane profile appears to be the result of a

different methane production–consumption balance at this depth, but has not been examined in detail.

Surface methane emission. The surface methane emission (F_S) was either measured using a flux chamber (all Northeast basin

values except on 20th June) or estimated from a wind-based model (all other values) that was developed from the flux chamber measurements and concurrent wind conditions. Emission data were transformed to gas transfer constants k_{600} as a linear function of wind speed (U_{10} , recorded at 10 m height), k_{600} [cm h^{-1}] = $1.98 * U_{10}$ [m s^{-1}] + 0.94 ($R^2 = 0.44$, $p < 0.01$). This linear function was then used to estimate surface emissions in the South basin (enclosures and open lake) based on wind speed (Supplementary Note 2, Supplementary Table 4). Other published models^{21,37,38} in the literature (mainly based on direct turbulence measurements)^{37,38} were used to validate these emission values (see sensitivity analysis in Discussion).

In the Northeast basin the surface methane emission increased by an order of magnitude from the non-stratified period (March: mean \pm SD; $0.049 \pm 0.026 \text{ mmol m}^{-2} \text{ d}^{-1}$) to the stratified period ($0.47 \pm 0.27 \text{ mmol m}^{-2} \text{ d}^{-1}$). Compared to the Northeast basin, higher surface emission was observed in the South basin during the stratified period (mean \pm SD; $0.71 \pm 0.24 \text{ mmol m}^{-2} \text{ d}^{-1}$).

The experimental enclosures showed a surface methane flux of (mean \pm SD) $0.43 \pm 0.07 \text{ mmol m}^{-2} \text{ d}^{-1}$ in August 2014, which was about half of the flux measured in the adjacent open water ($0.77 \text{ mmol m}^{-2} \text{ d}^{-1}$) at the same time. In contrast, the central reservoir showed a much lower surface methane emission of $0.01 \text{ mmol m}^{-2} \text{ d}^{-1}$ (measurement on 7th July). Details on flux parametrization are summarized in Supplementary Note 2.

Vertical methane diffusion. Diffusivity (K_z) was high in the SML, but it decreased to ca. $10^{-6} \text{ m}^2 \text{ s}^{-1}$ at the upper boundary of the thermocline in the stratified period (Supplementary Fig. 3c). Consequently, the diffusive methane input from the thermocline to the SML (F_z) during the stratified season was small for both the Northeast: (mean \pm SD) $0.032 \pm 0.031 \text{ mmol m}^{-2} \text{ d}^{-1}$ and the South basin: $0.050 \pm 0.065 \text{ mmol m}^{-2} \text{ d}^{-1}$, and negligible in the central reservoir ($4.4 \times 10^{-4} \text{ mmol m}^{-2} \text{ d}^{-1}$).

When the diffusive methane input was compared between experimental enclosures and open water in August 2014, the experimental enclosures showed lower values (mean \pm SD; $0.007 \pm 0.009 \text{ mmol m}^{-2} \text{ d}^{-1}$) than the adjacent open water ($0.024 \text{ mmol m}^{-2} \text{ d}^{-1}$).

Lateral input from littoral zones. Methane measurements were done in the experimental enclosures and the adjacent open water (South basin) in August 2014. The experimental enclosures were shielded from the littoral zone (e.g., no lateral methane input), therefore OMP in the SML was estimated from Eq. (1) (see Method section) without the F_L term to be (mean \pm SD) $101 \pm 17 \text{ nmol l}^{-1} \text{ d}^{-1}$ (Supplementary Table 5). By comparing the data from the experimental enclosures and those from the adjacent open water (both collected in the South basin) and deploying mass balance, we estimated the transport of methane from littoral sediments within the SML to the lake pelagic water to be $76 \pm 12 \text{ nmol l}^{-1} \text{ d}^{-1}$ (Supplementary Table 5), which corresponds to an average littoral sediment methane flux (F_L) of (mean \pm SD) $1.4 \pm 0.2 \text{ mmol m}^{-2} \text{ d}^{-1}$.

Oxic methane production. OMP at high temporal resolution (approximately weekly) in the two open-water sites was estimated from Eq. (1) (see Method section) using as F_L term (lateral methane input) the value obtained for August 2014 as described above. During the non-stratified season, OMP rates were negligible and then slowly increased in late April/May 2016 (Fig. 3). As the water column became fully stratified, the average OMP rate between the two basins ranged between 26 and $236 \text{ nmol l}^{-1} \text{ d}^{-1}$, reaching the maximum for both basins ($259 \text{ nmol l}^{-1} \text{ d}^{-1}$ in

Northeast basin, $214 \text{ nmol l}^{-1} \text{ d}^{-1}$ in South basin) in late June (Fig. 3).

Monte Carlo simulation was applied to assess uncertainties in the mass balance for the stratified period, and the resultant OMP rates in the SML were (mean \pm SD) $72 \pm 74 \text{ nmol l}^{-1} \text{ d}^{-1}$ (84% probability of positive value) for the Northeast basin and $88 \pm 75 \text{ nmol l}^{-1} \text{ d}^{-1}$ for the South basin (Table 1). On average, OMP contributed 64% of the surface methane emission in the Northeast basin, and 50% in the South basin, with the remaining methane originating from anoxic sources. A sensitivity analysis (see discussion) examined the effect of variable mass balance components on the contribution pattern.

Predicting oxic methane contribution from lake morphology.

Our analysis shows that lateral input from the littoral zone and in situ OMP were the two major SML methane sources, together accounting for $\geq 95\%$ of the surface emission in Lake Stechlin. While the estimated OMP rate was comparable between the two basins, its relative importance, expressed as the percentage of oxic methane contribution to the system-wide emission (OMC), was considerably higher in the Northeast basin than in the South basin. This difference was explained by the difference in geomorphology between the two basins: lateral input is a function of littoral sediment area (A_{sed}), whereas OMP is a function of the volume of SML across the lake basin (V). The relative importance between lateral input versus in situ OMP is therefore scaled to A_{sed}/V , which decreases with increasing basin size.

While Stechlin's Northeast and South basins vary in surface area (NE: 2.01 km^2 ; S: 1.12 km^2) and SML volume V (NE: $11,200,000 \text{ m}^3$; S: $5,700,000 \text{ m}^3$), their littoral sediment areas are comparable (NE: 0.28 km^2 , S: 0.31 km^2) (values given for a 6 m deep SML). As expected, OMC was higher in the larger Northeast basin (64%) compared to the smaller South basin (50%) due to a smaller A_{sed}/V ratio in the Northeast basin.

We extended this scaling exercise to other temperate oligo- to mesotrophic lakes of various sizes extracted from the literature^{21,32,39} (Supplementary Note 3, Supplementary Table 6) in order to derive an empirical relationship between OMC and lake morphology. The data showed that OMC is a negative log-linear function of A_{sed}/V (Fig. 4). Least square regression after linearization gave a highly significant p value ($\ll 0.01$) and a high R^2 value (0.95). A significant relationship was also found between OMC and lake surface area (Supplementary Fig. 6). Both functions predicted that the importance of OMP for SML methane increases with lake size; for lakes with $A_{\text{sed}}/V \leq 0.07 \text{ m}^2 \text{ m}^{-3}$ or surface area $\geq 1 \text{ km}^2$, OMP is expected to be the main source ($>50\%$) of surface methane emissions.

Discussion

In this study, we balanced the methane sources in two basins of the temperate meso-oligotrophic Lake Stechlin in high temporal resolution covering the shift from mixed to stratified water column conditions. We further analyzed the methane budget in two different types of enclosures, both isolated from littoral methane input: in experimental enclosures (1200 m^3) where water is periodically exchanged (last time 2 weeks prior to sampling) and in the central reservoir ($14,000 \text{ m}^3$) where water has not been exchanged since installation in 2011/2012 and is likely nutrient depleted. Comparing the methane budgets in the open water and enclosures allowed us to demonstrate that stratification mainly disconnected SML methane from bottom sediment methanogenesis, that OMP occurred irrespective of littoral influence, and that OMP contributed substantially to the system-wide methane emission of Lake Stechlin's Northeast (64%) and South basin (50%) exceeding the littoral methane source contribution (32% in

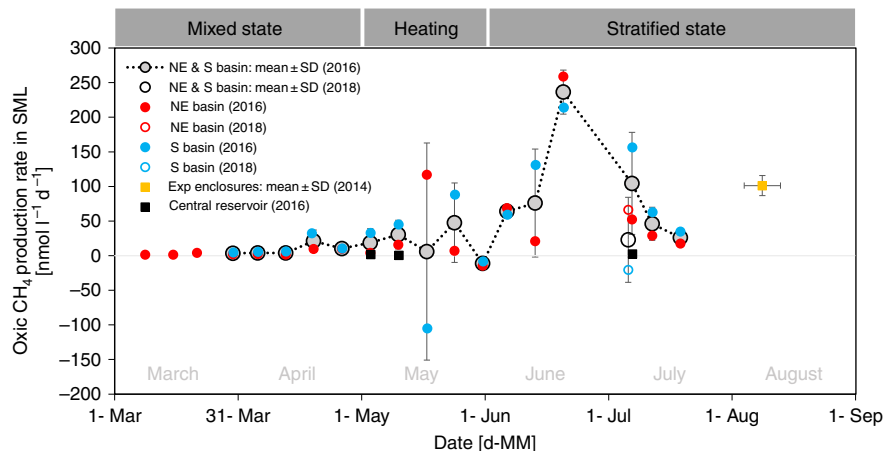


Fig. 3 Oxic methane production rates. Production rates were computed using a mass balance approach. Red circles represent measurements in the open water of the Northeast basin (69.5 m deep; 53°09'20.2"N 13°01'51.5"E) and blue circles measurements in the open water of the South basin (20.5 m deep; 53°08'36.6"N 13°01'42.8"E). Gray circles are average values of both basins. The yellow square is the average value for the experimental enclosures of the lake lab facility (enclosures 1 and 13), and black squares are measurements in the central reservoir. Vertical error bars illustrate standard deviation from mean values; and horizontal error bars (only experimental enclosures) depict the time frame of corresponding sampling. The mass balance was estimated for unstratified condition in March/April 2016 (negligible lateral methane flux, negligible methane oxidation) and for stratified condition June–August 2014/2016/2018 (lateral methane input from sediments: 1.4 mmol m⁻² d⁻¹; 30% of internally produced methane is oxidation). For May 2016, non-stratified parametrization was used for the first half of the month and stratified parametrization for the second half. Methane surface emission was measured in the Northeast basin (except on 20th June 2016) and on 6th July 2018 in the South basin, and was estimated for the other sites based on wind speed parametrization. The sampling schedule for all field measurements is laid out in Supplementary Table 3. Source data are provided as a Source Data file.

Table 1 Mass balance components.

Site	Mass balance component	Symbol	Whole system		Per volume
			[mol d ⁻¹]	[kg d ⁻¹]	[nmol l ⁻¹ d ⁻¹]
Northeast basin	Surface emission	F_S	942 ± 538	15 ± 9	90 ± 52
	Methane oxidation	MOx	226	4	22
	Lateral sediment input	F_L	372 ± 57	6 ± 1	36 ± 6
	Diffusion from thermocline	F_z	56 ± 55	1 ± 1	5 ± 5
	Internal (oxic) production	P_{net}	752 ± 771	12 ± 12	72 ± 74
South basin	Surface emission	F_S	795 ± 268	13 ± 4	148 ± 50
	Methane oxidation	MOx	141	2	26
	Lateral sediment input	F_L	423 ± 65	7 ± 1	79 ± 12
	Diffusion from thermocline	F_z	41 ± 54	1 ± 1	8 ± 10
	Internal (oxic) production	P_{net}	470 ± 400	8 ± 6	88 ± 75

Oxic production was computed by measuring/estimating surface emission, oxidation, lateral input, as well as vertical diffusion (see Fig. 1) and solving the mass balance for the missing component. Seven replicate measurements were taken in the open water of the Northeast (69.5 m deep; surface area 2,006,700 m²; 53°09'20.2"N 13°01'51.5"E) and South basin (20.5 m deep; surface area 1,122,775 m²; 53°08'36.6"N 13°01'42.8"E) of Lake Stechlin during the stratified period in 2016 (June–July). Values listed as mean ± SD. Note that Monte Carlo simulation was used to solve the mass balance after the target component (in bold; mean ± 1 SD) (see Methods for details). Supplementary Fig. 5 illustrates the density function of the Northeast and South basin dataset. If the Monte Carlo simulation were to be applied to whole lake data (combining South and Northeast basins data), oxic methane production rates (denoted as P_{net} in Eq. (1)) do not change: 78 ± 80 nmol l⁻¹ d⁻¹ (F_S = 2503 ± 1160, MOx = 496, F_L = 1198 ± 185, F_z = 139 ± 170, P_{net} = 1653 ± 1703 mol d⁻¹)

the Northeast basin and 45% in the South basin). Finally, combining mass balance results for Lake Stechlin and literature data for other lakes allowed us to develop a predictive model estimating the contribution of OMP to the system-wide methane surface emission as a function of lake morphological parameters, and the model suggests that OMP has important ramifications especially in large stratified lakes.

Mass balance approach has been successfully used by others to study methane dynamics in lakes⁴⁰, including OMP^{21,32}. However, this approach is sensitive to the accuracy of the individual components of the mass balance. Therefore, to assess the validity and robustness of our mass balance analysis, we evaluated the different components by comparing our measurements with literature values and examined how variabilities of the mass balance components may alter the overall

conclusion. The average surface methane emission (F_S) during the stratified period was 0.47 mmol m⁻² d⁻¹ (±57% SD) in the Northeast basin and 0.71 mmol m⁻² d⁻¹ (±34% SD) in the South basin (taken mainly during calm weather). The larger value in the South basin can be attributed to higher influence from littoral methane sources. However, these emission values are comparable with the global estimate of 0.62 mmol m⁻² d⁻¹ for the region 25–54° latitude⁴¹ and within the range reported earlier for Lake Stechlin⁴² (exceeding 4 mmol m⁻² d⁻¹ at strong wind; on average 2.6 mmol m⁻² d⁻¹ ± 42% SD). Highly variable surface emission has been reported earlier, for some systems standard deviations exceed 100% of mean emission values during summer^{24,26}. In case of the South basin we estimated the emission from wind speed data and the corresponding results are dependent on the gas transfer constant (k_{600}) value used.

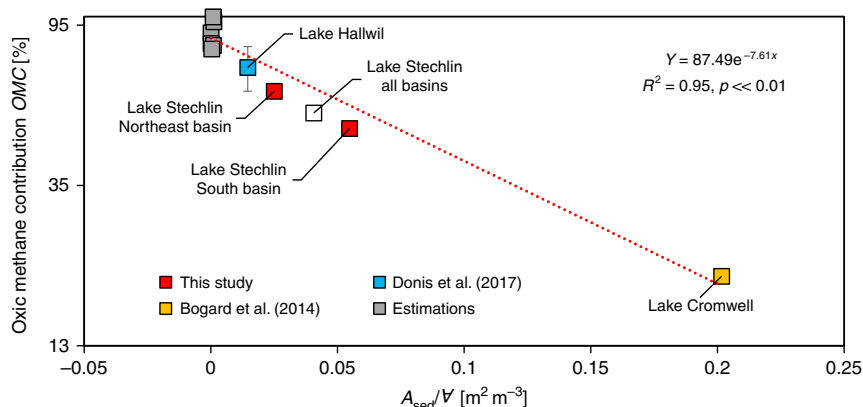


Fig. 4 Oxitic methane contribution versus lake morphology. The ratio of sediment area (A_{sed}) and surface mixed layer volume (V) determines the oxitic methane contribution to surface emission (OMC). The trend line (red line) follows the exponential function $y = 87.49e^{-7.61x}$ ($R^2 = 0.95$, $p \ll 0.01$, standard error = 8.6%). The y-axis is scaled to $\log_{2.7}$ and the x-axis is linear. With increasing lake size, V increases quicker than A_{sed} making oxitic methane production the largest source of surface mixed layer methane in lakes with $A_{\text{sed}}/V \leq 0.07 \text{ m}^2 \text{ m}^{-3}$. Lake Hallwil estimation²¹ was updated as described in Supplementary Note 1; the lower and upper end (error bars) were used to compute the mean OMC which was used for developing the trend line function. Estimations for other lakes were computed as defined in Supplementary Note 3. If whole lake data (combining South and Northeast basin data) was to be applied to this empirical model (empty symbol) the regression constants and statistics only change minimally ($y = 88.48e^{-7.56x}$; $R^2 = 0.96$, $p \ll 0.01$). Source data are provided as a Source Data file.

Our k_{600} -wind speed relationship ($k_{600} [\text{cm h}^{-1}] = 1.98 \times U_{10} [\text{m s}^{-1}] + 0.98$) was very similar to an earlier report (e.g., Lake Hallwil: $k_{600} [\text{cm h}^{-1}] = 2.0 \times U_{10} [\text{m s}^{-1}]$; Donis et al.²¹). Applying six alternative emission models (based on wind or combined wind and lake size) presented by Vachon and Prairie³⁷, MacIntyre et al.³⁸ and Donis et al.²¹ to this dataset resulted in an average emission rate between 0.55 and 1.03 $\text{mmol m}^{-2} \text{ d}^{-1}$. Applying these alternative emission rates to the mass balance analysis gave an OMP rate between 41 and 185 $\text{nmol l}^{-1} \text{ d}^{-1}$, which still translated to a substantial oxitic methane contribution (32–68%) to the surface methane emission (details in Supplementary Table 7). In other words, regardless of the method or model used to estimate surface methane emission, it remains that OMP was an important contributor to surface emission.

Comparing the methane data inside the experimental enclosures with that of the open water gave an average lateral methane input (F_L) of 1.4 $\text{mmol m}^{-2} \text{ d}^{-1}$ from the littoral sediment. It is within the range of fluxes reported for other temperate water bodies (e.g., Rzeszów Reservoir, Poland⁴³: (mean \pm SD) $0.69 \pm 0.56 \text{ mmol m}^{-2} \text{ d}^{-1}$ in May–Sep; Lake Hallwil, Switzerland²¹: $1.75 \pm 0.2 \text{ mmol m}^{-2} \text{ d}^{-1}$ in Sep (Supplementary Note 1); Boltzmann–Arrhenius equation at ca. 20 °C¹²: ca. $2 \text{ mmol m}^{-2} \text{ d}^{-1}$, including Lake Constance (Überlingen basin)/Lake Ammer/Lake Königsegg/Reservoir Schwarzbach in Germany¹² with ca. $1.3 \text{ mmol m}^{-2} \text{ d}^{-1}$). Even doubling the lateral methane input, what is an unlikely scenario for a meso-oligotrophic lake such as Lake Stechlin, still could not fully explain the observed SML methane in the Northeast basin, and a substantial OMP rate ($19 \text{ nmol l}^{-1} \text{ d}^{-1}$) would still be required to balance the methane budget. More importantly, within the experimental enclosures, which were isolated from lateral input, the estimated OMP was (mean \pm SD) $101 \pm 17 \text{ nmol l}^{-1} \text{ d}^{-1}$ (Aug 2014 dataset), which was comparable to the estimated average OMP in the open water for both basins ($72\text{--}88 \text{ nmol l}^{-1} \text{ d}^{-1}$) (June/July 2016 dataset).

The calculation of methane diffusive input from the lower water layers (F_z) is dependent on the estimated K_z value (diffusivity). Our K_z values were comparable to an earlier report for the same lake³⁶. Even in Lake Hallwil, which is 5–10 times larger than the Lake Stechlin basins and is therefore exposed to stronger seiche effects, very similar K_z values were observed²¹

(thermocline minimum about $10^{-6} \text{ m}^2 \text{ s}^{-1}$). The SML methane in Lake Stechlin was decoupled from bottom sediment methanogenesis during thermal stratification, as it is also indicated by the methane-depth profile of the central reservoir (Fig. 2e) where water has not been exchanged since installation in 2011/2012. Accordingly, methane diffusion from Lake Stechlin’s thermocline water accounted for only 2–5% (likely overestimated) of the SML methane in the open-water sites, and only 1% in the experimental enclosures. Variability in the corresponding mass balance components, therefore, was negligible and would not affect the overall conclusion.

The magnitude of methane oxidation (MOx) varies between seasons^{44–46} and between lakes³⁹. Oxygen concentration⁴⁷ and light^{48,49} are important modulating factors for MOx in lake surface waters. In other lakes, MOx rates in oxitic surface waters have been reported to range between 4 and 30 $\text{nmol l}^{-1} \text{ d}^{-1}$ ^{21,32,50}. For our study, we assumed MOx to be equivalent to a constant fraction (30%) of the internal production during the stratified season (see method section for details). The average OMP rates for both basins were $72\text{--}88 \text{ nmol l}^{-1} \text{ d}^{-1}$, giving a hypothetical MOx rate of ca. $24 \text{ nmol l}^{-1} \text{ d}^{-1}$, which is within the range of literature values. Because methane oxidation is parameterized as a loss term in the mass balance analysis, higher MOx would translate to higher OMP, and vice versa. If we consider the extreme scenario by completely ignoring methane oxidation ($MOx = 0$), the estimated average OMP rate for the South basin would decrease to (mean \pm SD) $40 \pm 53 \text{ nmol l}^{-1} \text{ d}^{-1}$ and would still remain an important SML methane source (32%).

Comparing our measurements and assumptions against literature values shows that our mass balance analysis is reasonably parameterized and robust. The system-wide methane emission from the SML in the Northeast basin was estimated to be 942 mol d^{-1} in the stratified period, of which 32% from lateral input (372 mol d^{-1}) and 5% from vertical diffusion from the thermocline (56 mol d^{-1}) (Table 1). Similarly, methane emission from the SML in the South basin was 795 mol d^{-1} , and only 45% (423 mol d^{-1}) could be attributed to lateral input and 4% (41 mol d^{-1}) to vertical input from the thermocline. The deficits (plus additional consumption via methanotrophy), therefore, must be compensated for by internal OMP. The estimated OMP rate averaged over the stratified period was (mean \pm SD) $72 \pm 74 \text{ nmol l}^{-1} \text{ d}^{-1}$ (Northeast basin) and $88 \pm$

75 nmol l⁻¹ d⁻¹ (South basin). An earlier study¹⁵ using bottle incubations measured a net OMP rate of up to 58 nmol l⁻¹ d⁻¹ for Lake Stechlin, which corresponds to a hypothetical gross production rate of 75 nmol l⁻¹ d⁻¹ when assuming 30% oxidation. Similar OMP rates have also been estimated for Lake Hallwil, between 76 and 138 nmol l⁻¹ d⁻¹²¹ (Supplementary Note 1). Particularly high OMP values, such as what we found in late June (mean ± SD; 236 ± 32 nmol l⁻¹ d⁻¹), have also been reported by others³² (e.g., 230 ± 10 nmol l⁻¹ d⁻¹ in Lake Cromwell, Canada). Overall, by accounting for the different methane sources and sinks in the SML mass balance analysis, we show that OMP is a key contributor to system-wide surface emission in Lake Stechlin. This conclusion is consistent with previously reported OMP rates obtained from bottle incubations¹⁵ and is not sensitive to inherent uncertainties in our mass balance approach as shown by the sensitivity analysis.

In addition to known knowledge gaps in the global methane dynamics^{22,23}, OMP has not been considered as source of uncertainty in global assessments^{1,2,22,23}. Because both oxic and anoxic methane sources in lakes can be modulated by multiple factors and processes (Supplementary Fig. 7), some of which are still poorly understood, it would be premature to construct a mechanistic model to fully describe methane dynamics in lakes. Instead, we developed empirical models as useful tools to predict the contribution of OMP to the system-wide emission (*OMC*) in stratified meso-to-oligotrophic lakes in the temperate region based on a set of simple lake morphological parameters (Fig. 4, Supplementary Fig. 6). The first model using littoral sediment area (A_{sed}) and SML volume (\forall) as proxy explains nearly the entire variance in the dataset ($R^2 = 0.95$, $p \ll 0.01$) making it a powerful predictive model to estimate *OMC* from A_{sed} and \forall . For cases where A_{sed} and \forall data are unavailable, *OMC* can be related to easily accessible lake surface area (Supplementary Fig. 6). With an average accuracy of 91.4% (standard error = 8.6%) this model also provides reliable *OMC* estimates. Both empirical models predict the importance of OMP for atmospheric emission to increase with lake size.

The system-wide contribution of the anoxic methane sources is mainly controlled by littoral sediment flux and the corresponding littoral sediment area. Trophic state^{51,52} and temperature^{12,53} are important drivers of the methane flux from sediments. Higher sediment methane fluxes in eutrophic systems and in warmer climate zones compared to our dataset of stratified meso-to-oligotrophic lakes in the temperate region could shift the curve of the empirical models to the right (Fig. 4, Supplementary Fig. 6). However, sediment methane fluxes vary in a rather narrow range by a factor of 26 between oligotrophic and eutrophic lakes⁵² (e.g., 0.2–5.2 mmol m⁻² d⁻¹). Likewise, reported average OMP rates varied by a factor of 6 in stratified lakes^{15,21,32} (40–230 nmol l⁻¹ d⁻¹ including this study). In comparison, our predictive model covers lake surface area that varies by a factor of 190,000. The *OMC* prediction, therefore, may vary mainly for small lakes which have been reported to cause less methane emission on a global scale compared to large lakes²⁸ (<0.01 versus >1 km²). It shall be noted that the model predictions based on A_{sed} and \forall will be more reliable than based exclusively on lake surface area due to sediment steepness, aspect ratio and total depth modulating the littoral sediment area at constant lake surface area.

Methane emission from lakes has been identified as a key contributor of this powerful greenhouse gas to the atmosphere²². It is therefore a legitimate question to ask: how important is OMP in this context on a global scale? To get a first-order estimation, we applied our empirical model to the global lake size distributions based on satellite data, which covers lakes ≥ 0.01 km²²³¹. The result suggests that globally, an average of 66% of lake methane emission may have originated from oxic production

(Supplementary Note 4, Supplementary Table 8). Such a surprising finding justifies the need for further investigation of OMP in lakes worldwide with different geological histories, trophic states, climates, and physical (e.g., lake color, stratification patterns or with strong in-/out flow) and chemical characteristics (e.g., alkaline versus acidic) (Supplementary Fig. 7). By increasing data resolution in our empirical models, the models can then be used to further improve the global methane emission assessments.

Unlike the anoxic methane production driven by anaerobic methanogens with enzymes that are oxygen-sensitive⁵⁴, OMP in lake waters has been attributed to novel biochemical pathways involving photoautotrophs^{15,34,55}. Our system-wide methane mass balance demonstrates that without OMP a substantial methane source is missing when balancing Lake Stechlin's SML methane sources and sinks. The estimated OMP rates agree very well with earlier results from bottle incubation experiments¹⁵ and account for $\geq 50\%$ of the system-wide methane emission. Following our model, *OMC* is predicted to be the major methane source for the system-wide emission in lakes >1 km². In the light of global warming and widespread lake eutrophication, stratification periods will extend^{56,57} and phytoplankton production in the SML is expected to increase worldwide⁵⁸, which may increase OMP and its contribution to methane emission to the atmosphere. To understand and predict future climate change scenarios, it is crucial to consider lake water OMP in the global methane assessment and how it responds to environmental perturbations.

Methods

Study site. Lake Stechlin (Germany) is a meso-oligotrophic temperate glacial lake. For this study, we focused on the Northeast and South basins. Typical of temperate lakes, the water column of Lake Stechlin is well mixed in winter, begins to stratify in April/May and remains stratified until September or October. Throughout the stratified period, the oxygen-rich SML and thermocline are oversaturated with methane^{19,34}.

The Lake Lab facility was installed in the South basin in 2011/2012, which consists of 24 experimental enclosures (each 9 m diameter × 20 m depth) and a central reservoir (30 m diameter × 20 m depth), all of which extend into the bottom sediment. Water in the experimental enclosures 1 and 13 of the Lake Lab facility was exchanged with open lake water 2 weeks prior to our study; the water in the central reservoir has never been changed since installation.

Parameters of lake morphology, such as volume of the SML (\forall) and planar areas (A_{tot} , A_{th} , A_{sed}), were derived from thermocline depth data and bathymetry data. Supplementary Table 9 summarizes the parameterization of the mass balance for open-water and enclosure calculations for the stratified (June–July 2016/2018; Aug 2014) and the non-stratified periods (March–April 2016).

Mass balance analysis. The mass balance analysis examines the different processes leading to methane gains and losses within the SML (Fig. 1). The gains include horizontal transport from the shore, vertical diffusion from the thermocline, river input and internal production (OMP). The losses are methane oxidation and surface emission and river outflow.

We used the following mass balance equation and solved either for oxic methane production, P_{net} (= OMP), or lateral methane input, F_L ²¹

$$\frac{\partial C}{\partial t} * \forall = (Q_R * C_R) + (Q_C * C_C) + (A_{\text{th}} * F_z) + (A_{\text{sed}} * F_L) + (P_{\text{net}} * \forall) - (MOx * \forall + A_{\text{tot}} * F_S) \quad (1)$$

Here, $\frac{\partial C}{\partial t}$ describes the changing methane concentration over time [mol m⁻³ d⁻¹] (which under steady state condition is simplified to $\frac{\partial C}{\partial t} = 0$), \forall is the volume of the surface mixed volume [m³]. ($Q_R \times C_R$) and ($Q_C \times C_C$) describes optional methane input and output by river in- and outflow where Q_R (Q_C) is the flowrate [m³ d⁻¹] and C_R (C_C) is the methane concentration of inflowing (outflowing) water [mol m⁻³]. The term ($A_{\text{th}} \times F_z$) describes the vertical methane input from below via interior turbulent diffusion: F_z [mol m⁻² d⁻¹] (z is the depth in a 1-m resolution) multiplied by the thermocline area A_{th} [m²]. The term ($A_{\text{sed}} \times F_L$) describes lateral methane input from sediments with A_{sed} being the surface area of the littoral sediment [m²] and F_L being the sediment methane flux [mol m⁻² d⁻¹]. P_{net} is the local methane production rate per unit SML volume [mol m⁻³ d⁻¹]. Methane loss terms include local oxidation rate (MOx ; [mol m⁻³ d⁻¹]) and emission to the atmosphere ($A_{\text{tot}} \times F_S$; where A_{tot} is the lakes' surface area [m²] and F_S is the surface emission [mol m⁻² d⁻¹]). Note that P_{net} symbolizes oxic methane production

which is abbreviated in the running text as OMP. The mass balance was parametrized accordingly (Supplementary Table 9).

Monte Carlo simulation. To assess uncertainties, Monte Carlo simulation was used (9999 iterations) when solving the mass balance. Using the $rnorm$ -function of R^{59,60}, mass balance components were randomly picked within the normal distribution resulting from mean values (μ) and their standard deviations $\sigma =$

$\sqrt{\left(\frac{\sum(x - \bar{x})^2}{(n - 1)}\right)}$ retrieved from field measurements. Here, the normal distribution has the density $f(x) = (1/\sqrt{2\pi}\sigma)e^{-((x-\mu)^2/(2\sigma^2))}$. Mass balance output is presented as mean $\pm 1\sigma$.

Methane concentration. In two experimental enclosures (1, 13) and the adjacent open-water in the South basin, methane concentration within the top 18 m of the water column was sampled in a 1-m resolution 4–5 times over 10 days in August 2014. Weekly water column profile sampling was also carried out between 10:00 and 18:00 local time, from March to July in 2016 at the open-water sites in the Northeast basin (69.5 m deep) and in the South basin (20.5 m deep). In July 2018, one additional profile measurement was taken in both basins. Furthermore, the central reservoir was sampled on three occasions in 2016 (on 3rd and 10th May when stratification was developing, and on 7th July when the water was fully stratified). Water was collected from different depths by a Limnos Water Sampler, and gently transferred to 50 ml serum bottles via a tubing. The bottles were fully flushed three times, filled and crimp-closed with PTFE-butyl septa (triplicates at the Northeast basin, duplicates elsewhere). Dissolved methane concentrations were measured in the lab by headspace displacement method and a GC/FID⁶¹ (Shimadzu).

Surface methane emission. Methane surface emission (F_S) was captured by a 15 l-volume floating chamber. Trapped methane was quantified by withdrawing the gas from the chamber and measuring it by headspace analysis (GC/FID). Emission data were then used to derive gas transfer constant (k_{600}) as a function of wind speed at 10 m height (U_{10}) (Supplementary Note 2). For times when we did not have direct emission measurements, we used the k_{600} -relationship to estimate methane emissions based on wind speed. Parameters computed for flux estimations are summarized in Supplementary Table 4.

Lateral methane input. To estimate how much methane was introduced from littoral sediments into the SML during the stratified period, methane measurements were taken inside mesocosm enclosures (2 weeks after the water was exchanged with open lake water) and in the open water adjacent to the enclosures in the South basin (details in Supplementary Table 3). As the enclosures were cut off from lateral transport, by comparing the mass balance analysis results between inside and outside of the enclosures, we were able to derive the lateral methane input.

We neglected lateral methane input for the non-stratified season as sediment methanogenesis is highly temperature dependent^{62,63} and was observed to be zero or 1–2 orders of magnitude smaller under winter conditions compared to summer/autumn condition^{62,64,65}.

Vertical methane diffusion. The stratified period (June–July) was characterized by a distinct methane peak in the thermocline. To estimate the transport of methane from the thermocline into the SML via (turbulent) diffusion, we applied the Fick's First law as follows

$$F_z = -K_z * \frac{\partial C}{\partial z}; [\text{mol m}^{-2} \text{d}^{-1}], \quad (2)$$

where F_z is the average vertical methane diffusion, z is depth [m], $\frac{\partial C}{\partial z}$ is the vertical methane gradient measured at 1-m depth resolution, and K_z is the basin-scale diffusivity [$\text{m}^2 \text{s}^{-1}$] derived from temperature data based on the heat-budget method (Supplementary Note 5, Supplementary Fig. 3c). To obtain a conservative estimate of OMP in the SML, maximum K_z values within the bottom 3 m of the SML were used to compute F_z . Temperature and diffusivity profiles measured inside the mesocosms were very similar to the open-water profiles allowing us to apply the same heat-budget estimates of open-water diffusivity values at depths >4 m to estimate the vertical flux in both open lake and mesocosm enclosures for the entire study period (Supplementary Fig. 8).

Methane oxidation. Methane oxidation (MOx) rates of up to $103 \text{ nmol l}^{-1} \text{ d}^{-1}$ have been observed in Lake Stechlin, when water was spiked with high methane concentrations¹⁶. However, MOx rate in lake waters has been observed to differ by 1–2 orders of magnitude between winter and summer^{45–47}. For a more conservative consideration (MOx is a loss term in the mass balance) and to account for the seasonal difference and to simplify our mass balance analysis, we neglected MOx for the non-stratified season, and we assumed

MOx to be 30% of the internal production rate during the stratified season. We evaluated this assumption in a sensitivity analysis in the discussion section.

River connection and ebullition. Lake Stechlin is not connected to any river. Therefore, the corresponding mass balance terms ($Q_R \times C_R$) and ($Q_C \times C_C$) equal 0. No methane ebullition was observed during the whole study period. Earlier studies reported generally low methanogenesis activity in Lake Stechlin sediments^{66–68}, with the majority occurring below 20 cm sediment depth⁶⁹. Tang et al.¹⁶ demonstrated that ebullition did not contribute methane to SML waters for depths ≥ 20 m. This allowed us to ignore ebullition in our mass balance analysis for Lake Stechlin (22.7 m mean depth).

Environmental parameters. Water depths were measured by a portable sounder gauge (Cole-Parmer). Temperature, dissolved oxygen and chlorophyll fluorescence was measured using a YSI probe (Model 6600V2). Wind speed data (U_{10} recorded at 10 m height) were provided in 30–60 min resolution by the Neuglobsow weather station (Federal Environmental Agency) adjacent to the lake.

Oxic methane contribution. We examined the importance of oxic methane production relative to anoxic sources (lateral input, vertical diffusion) by computing the OMC

$$OMC = (P_{\text{net}} * \forall) * 100 / ((P_{\text{net}} * \forall) + (A_{\text{sed}} * F_L) + (A_{\text{th}} * F_z)); [\%]. \quad (3)$$

We then compared our results with the literature data^{21,32} (Supplementary Note 3) to examine OMC as a function of lake morphology. To expand our analysis to larger lakes, we estimated OMC for additional lakes based on the data in DelSontro et al.³⁹ (Supplementary Note 3, Supplementary Table 6).

Data format. This study contains multiple field samplings done in the course of 2014, 2016, and 2018. Mean ± 1 standard deviations presented throughout the manuscript indicate temporal variation and were calculated separately for the stratified/non-stratified season for each basin or combined for the experimental enclosures or the central reservoir. R^2 values presented throughout the paper are based on LM models.

Reporting summary. Further information on experimental design is available in the Nature Research Reporting Summary linked to this paper.

Data availability

Data are made available in graphical or tabular form throughout the paper and Supplementary Information. The source data underlying Figs. 2–4 and Supplementary Figs. 1, 3, 4, 5, 6, and 8 are provided as a Source Data file.

Received: 27 April 2019; Accepted: 30 October 2019;

Published online: 02 December 2019

References

- Solomon, S. et al. *Climate Change 2007: The Physical Science Basis. Contribution of Working Group I to the Fourth Assessment Report of the Intergovernmental Panel on Climate Change.* (Cambridge University Press, Cambridge, New York, 2007).
- Stocker, T. F. et al. *Climate Change 2013: The Physical Science Basis. Contribution of Working Group I to the Fifth Assessment Report of the Intergovernmental Panel on Climate Change.* (Cambridge University Press, Cambridge, New York, 2013).
- Nisbet, E. G. et al. Very strong atmospheric methane growth in the 4 years 2014–2017: implications for the Paris Agreement. *Glob. Biogeochem. Cycles* **33**, 318–342 (2019).
- Mikaloff-Fletcher, S. E. & Schaefer, H. Rising methane: A new climate challenge. *Science* **364**, 932–933 (2019).
- Thauer, R. K. Biochemistry of methanogenesis: a tribute to Marjory Stephenson: 1998 Marjory Stephenson Prize Lecture. *Microbiology* **144**, 2377–2406 (1998).
- Ferry, J. G. & Kastead, K. A. Methanogenesis. in *Archaea: Molecular and Cellular Biology* (ed. Cavicchioli, R.) 288–314 (ASM Press, Washington DC, 2007).
- Scranton, M. I. & Brewer, P. G. Occurrence of methane in the near-surface waters of the western subtropical North-Atlantic. *Deep Sea Res.* **24**, 127–138 (1977).
- Tang, K. W., McGinnis, D. F., Ionescu, D. & Grossart, H.-P. Methane production in oxic lake waters potentially increases aquatic methane flux to air. *Environ. Sci. Technol. Lett.* **3**, 227–233 (2016).

9. Murase, J., Sakai, Y., Kametani, A. & Sugimoto, A. Dynamics of methane in mesotrophic Lake Biwa, Japan. *Ecol. Res.* **20**, 377–385 (2005).
10. Hofmann, H., Federwisch, L. & Peeters, F. Wave-induced release of methane: littoral zones as source of methane in lakes. *Limnol. Oceanogr.* **55**, 1990–2000 (2010).
11. Fernandez, J. E., Peeters, F. & Hofmann, H. On the methane paradox: transport from shallow water zones rather than in situ methanogenesis is the major source of CH₄ in the open surface water of lakes. *J. Geophys. Res. Biogeosci.* **121**, 2717–2726 (2016).
12. Peeters, F., Fernandez, J. E. & Hofmann, H. Sediment fluxes rather than oxic methanogenesis explain diffusive CH₄ emissions from lakes and reservoirs. *Sci. Rep.* **9**, 243 (2019).
13. Karl, D. M. et al. Aerobic production of methane in the sea. *Nat. Geosci.* **1**, 473–478 (2008).
14. Damm, E. et al. Methane production in aerobic oligotrophic surface water in the central Arctic Ocean. *Biogeosciences* **7**, 1099–1108 (2010).
15. Grossart, H.-P., Frindte, K., Dziallas, C., Eckert, W. & Tang, K. W. Microbial methane production in oxygenated water column of an oligotrophic lake. *Proc. Natl Acad. Sci. USA* **108**, 19657–19661 (2011).
16. Tang, K. W., McGinnis, D. F., Frindte, K., Brüchert, V. & Grossart, H.-P. Paradox reconsidered: methane oversaturation in well-oxygenated lake waters. *Limnol. Oceanogr.* **59**, 275–284 (2014).
17. Yao, M., Henny, C. & Maresca, J. A. Freshwater bacteria release methane as a by-product of phosphorus acquisition. *Appl. Environ. Microbiol.* **82**, 6994–7003 (2016).
18. Wang, Q., Dore, J. E. & McDermott, T. R. Methylphosphonate metabolism by *Pseudomonas* sp. populations contributes to the methane oversaturation paradox in an oxic freshwater lake. *Environ. Microbiol.* **19**, 2366–2378 (2017).
19. Bizic-Ionescu, M., Ionescu D., Günthel, M., Tang, K. W. & Grossart H.-P. Oxic Methane Cycling: New Evidence for Methane Formation in Oxic Lake Water. in *Biogenesis of Hydrocarbons* (eds. Stams, A. & Sousa, D.) 379–400 (Springer, Cham, 2018).
20. Carini, P., White, A. E., Campbell, E. O. & Giovannoni, S. J. Methane production by phosphate-starved SAR11 chemoheterotrophic marine bacteria. *Nat. Commun.* **5**, 4346 (2014).
21. Donis, D. et al. Full-scale evaluation of methane production under oxic conditions in a mesotrophic lake. *Nat. Commun.* **8**, 1661 (2017).
22. Saunio, M. et al. The global methane budget 2000–2012. *Earth Syst. Sci. Data* **8**, 697–751 (2016).
23. Kirschke, S. et al. Three decades of global methane sources and sinks. *Nat. Geosci.* **6**, 813–823 (2013).
24. Sabrekov, A. F. et al. Variability in methane emission from West Siberia's shallow boreal lakes on a regional scale and its environmental controls. *Biogeosciences* **14**, 3715–3742 (2017).
25. Natchimuthu, S. et al. Spatio-temporal variability of lake CH₄ fluxes and its influence on annual whole lake emission estimates. *Limnol. Oceanogr.* **61**, S13–S26 (2016).
26. Xiao, Q. et al. Spatial variation of methane emission in a large shallow eutrophic lake in subtropical climate. *J. Geophys. Res. Biogeosci.* **122**, 1597–1614 (2017).
27. Wik, M., Thornton, B. F., Bastviken, D., Uhlbäck, J. & Crill, P. M. Biased sampling of methane release from northern lakes: a problem for extrapolation. *Geophys. Res. Lett.* **43**, 1256–1262 (2016).
28. Bastviken, D., Cole, J., Pace, M. & Tranvik, L. Methane emission from lakes: dependence of lake characteristics, two regional assessments, and a global estimate. *Glob. Biogeochem. Cycles* **18**, GB4009 (2004).
29. Allen, G. H. & Pavelsky, T. M. Global extent of rivers and streams. *Science* **361**, 585–588 (2018).
30. Thornton, B. F., Wik, M. & Crill, P. M. Double-counting challenges the accuracy of high-latitude methane inventories. *Geophys. Res. Lett.* **43**, 12569–12577 (2016).
31. Cael, B. B., Heathcote, A. J. & Seekell, D. A. The volume and mean depth of Earth's lakes. *Geophys. Res. Lett.* **44**, 209–218 (2017).
32. Bogard, M. J. et al. Oxic water column methanogenesis as a major component of aquatic CH₄ fluxes. *Nat. Commun.* **5**, 5350 (2014).
33. Dean, J. F. et al. Methane feedbacks to the global climate system in a warmer world. *Rev. Geophys.* **56**, 207–250 (2018).
34. Bizic-Ionescu M. et al. Widespread formation of methane by *Cyanobacteria* in aquatic and terrestrial ecosystems. Preprint at *bioRxiv* <https://www.biorxiv.org/content/10.1101/398958v1> (2019).
35. Kirillin, G., Phillip, W., Engelhardt, C. & Nützmann, G. Net groundwater inflow in an enclosed lake: from synoptic variation to climatic projections. *Hydrol. Process.* **27**, 347–359 (2012).
36. Kirillin, G., Grossart, H.-P. & Tang, K. W. Modeling sinking rate of zooplankton carcasses: effects of stratification and mixing. *Limnol. Oceanogr.* **57**, 881–894 (2012).
37. Vachon, D. & Prairie, Y. T. The ecosystem size and shape dependence of gas transfer velocity versus wind speed relationships in lakes. *Can. J. Fish. Aquat. Sci.* **70**, 1757–1764 (2013).
38. MacIntyre, S. et al. Buoyancy flux, turbulence, and the gas transfer coefficient in a stratified lake. *Geophys. Res. Lett.* **37**, L24604 (2010).
39. DelSontro, T., del Giorgio, P. A. & Prairie, Y. T. No longer a paradox: the interaction between physical transport and biological processes explains the spatial distribution of surface water methane within and across lakes. *Ecosystems* **21**, 1073–1087 (2018).
40. Bastviken, D., Ejlertsson, J. & Tranvik, L. Measurement of methane oxidation in lakes: a comparison of methods. *Environ. Sci. Technol.* **36**, 3354–3361 (2002).
41. Bastviken, D., Tranvik, L. J., Downing, J. A., Crill, P. M. & Enrich-Prast, A. Freshwater methane emission offset the continental carbon sink. *Science* **331**, 50 (2011).
42. McGinnis, D. et al. Enhancing surface methane fluxes from an oligotrophic lake: exploring the microbubble hypothesis. *Environ. Sci. Technol.* **49**, 873–880 (2014).
43. Gruca-Rokosy, R. & Tomaszek, J. A. Methane and carbon dioxide in the sediment of a eutrophic reservoir: production pathways and diffusion fluxes at the sediment–water interface. *Water Air Soil Pollut.* **226**, 16 (2015).
44. Utsumi, M. et al. Oxidation of dissolved methane in a eutrophic, shallow lake: Lake Kasumigaura, Japan. *Limnol. Oceanogr.* **43**, 471–480 (1998).
45. Joye, S. B., Connell, T. L., Miller, L. G., Oremland, R. S. & Jellison, R. S. Oxidation of ammonia and methane in an alkaline, saline lake. *Limnol. Oceanogr.* **44**, 178–188 (1999).
46. Carini, S., Bano, N., LeClerc, G. & Joye, S. B. Aerobic methane oxidation and methanotroph community composition during seasonal stratification in Mono Lake, California (USA). *Environ. Microbiol.* **7**, 1127–1138 (2005).
47. Rudd, J. W. M., Furutani, A., Flett, R. J. & Hamilton, R. D. Factors controlling methane oxidation in shield lakes: the role of nitrogen fixation and oxygen concentration. *Limnol. Oceanogr.* **21**, 357–364 (1976).
48. Murase, J. & Sugimoto, A. Inhibitory effect of light on methane oxidation in the pelagic water column of a mesotrophic lake (Lake Biwa, Japan). *Limnol. Oceanogr.* **50**, 1339–1343 (2005).
49. Dumestre, J. F. et al. Influence of light intensity on methanotrophic bacterial activity in Petit Saut Reservoir, French Guiana. *Appl. Environ. Microbiol.* **65**, 534–539 (1999).
50. Oswald, K. et al. Light-dependent aerobic methane oxidation reduces methane emissions from seasonally stratified lakes. *PLoS ONE* **10**, e0132574 (2015).
51. Beaulieu, J. J., DelSontro, T. & Downing, J. A. Eutrophication will increase methane emission from lakes and impoundments during the 21st century. *Nat. Commun.* **10**, 1375 (2019).
52. Adams, D. D. Diffuse Flux of Greenhouse Gases - Methane and Carbon Dioxide - at the Sediment-Water Interface of Some Lakes and Reservoirs of the World. In *Greenhouse Gas Emissions—Fluxes and Processes. Hydroelectric Reservoirs and Natural Environments* (eds. Tremblay, A., Varfalvy, L., Roehm, C. & Garneau, M.) 129–153 (Springer, Berlin, Heidelberg, 2005).
53. Aben, R. C. H. et al. Cross continental increase in methane ebullition under climate change. *Nat. Commun.* **8**, 1682 (2017).
54. Jarrell, K. F. Extreme oxygen sensitivity in methanogenic archaeobacteria. *BioScience* **35**, 298–302 (1985).
55. Lenhart, K. et al. Evidence for methane production by the marine algae *Emiliania huxleyi*. *Biogeosciences* **13**, 3163–3174 (2016).
56. De Stasio, B. T. Jr., Hill, D. K., Kleinhans, J. M., Nibbelink, N. P. & Magnuson, J. J. Potential effects of global climate change on small north-temperate lakes: physics, fish, and plankton. *Limnol. Oceanogr.* **41**, 1136–1149 (1996).
57. Peeters, F., Straile, D., Lorke, A. & Livingstone, D. M. Earlier onset of the spring phytoplankton bloom in lakes of the temperate zone in a warmer climate. *Glob. Change Biol.* **13**, 1898–1909 (2007).
58. Visser, P. M. et al. How rising CO₂ and global warming may stimulate harmful cyanobacterial blooms. *Harmful Algae* **54**, 145–159 (2016).
59. R Core Team. *R (v3.3.1): A Language and Environment for Statistical Computing*. (R Foundation for Statistical Computing, Vienna, Austria, 2016). <https://www.R-project.org/>.
60. RStudio Team. *RStudio (v1.0.153): Integrated Development for R*. (RStudio, Inc., Boston, MA, 2016). <http://www.rstudio.com/>.
61. Magen, C. et al. A simple headspace equilibration method for measuring dissolved methane. *Limnol. Oceanogr. Methods* **12**, 637–650 (2014).
62. Duc, N. T., Crill, P. & Bastviken, D. Implications of temperature and sediment characteristics on methane formation and oxidation in lake sediments. *Biogeochemistry* **100**, 185–196 (2010).
63. Marotta, H. et al. Greenhouse gas production in low-latitude lake sediments responds strongly to warming. *Nat. Clim. Change* **4**, 467–470 (2014).
64. Liikanen, A. et al. Spatial and seasonal variation in greenhouse gas and nutrient dynamics and their interactions in the sediments of a boreal eutrophic lake. *Biogeochemistry* **65**, 83–103 (2003).

65. Liu, X., Gao, Y., Zhang, Z., Luo, J. & Yan, S. Sediment-water methane flux in a eutrophic pond and primary influential factors at different time scales. *Water* **9**, 601 (2017).
66. Casper, P., Furtado, A. L. S. & Adams, D. D. Biogeochemistry and diffuse fluxes of greenhouse gases (methane and carbon dioxide) and dinitrogen from the sediments of oligotrophic Lake Stechlin, Northern Germany. *Arch. Hydrobiol. Spec. Issues Adv. Limnol.* **58**, 53–71 (2003).
67. Casper, P. et al. Greenhouse gas cycling in aquatic ecosystems—methane in temperate lakes across an environmental gradient in northeast Germany. *Verh. Int. Ver. Limnol.* **29**, 564–566 (2005).
68. Conrad, R., Chan, O.-C., Claus, P. & Casper, P. Characterization of methanogenic Archaea and stable isotope fractionation during methane production in the profundal sediment of an oligotrophic lake (Lake Stechlin, Germany). *Limnol. Oceanogr.* **52**, 1393–1406 (2007).
69. Casper, P. Methane production in littoral and profundal sediments of an oligotrophic and a eutrophic lake. *Arch. Hydrobiol. Spec. Issues Adv. Limnol.* **48**, 253–259 (1996).

Acknowledgements

We thank Anke Penzlin and Marcus Wallasch (Umweltbundesamt, Germany) kindly provided weather data, Peter Casper (Leibniz Institute, Germany) for giving access to a GC/FID unit and the Lake Lab team (Leibniz Institute, Germany) for giving access to the Lake Lab enclosures and automated profiler data. Further thanks to Matthew Bogard (University of Washington Seattle, USA) for providing morphology parameters of Lake Cromwell and Tonya DelSontro (University of Geneva, Switzerland) for providing lake data for OMC estimations. Funding was provided by the Swiss National Science Foundation for D.F.M. and D.D. (grant 200021_169899), by the German Research Foundation for G.K. (KI-853/7-1, KI-853/11-1, KI-853/11-2). D.I., M.B. and H.P.G. were funded by the German Research Foundation (DFG; GR1540/21-1+2, 23-1, 28-1, BI1987/2-1), the German Federal Ministry of Education and Research (BMBF 01LC1501G) and the European Commission/ Horizon program (H2020 project ERA-PLANET).

Author contributions

M.G., H.-P.G., K.W.T., D.F.M., D.D. and G.K. contributed to the design of the study. M.G., H.-P.G., D.I. and M.B. collected the data; M.G. analyzed the data with input

from D.F.M., D.D. and G.K.; M.G. and K.W.T. wrote the paper with input from all co-authors.

Competing interests

The authors declare no competing interests.

Additional information

Supplementary information is available for this paper at <https://doi.org/10.1038/s41467-019-13320-0>.

Correspondence and requests for materials should be addressed to M.G., D.F.M., H.-P.G. or K.W.T.

Peer review information *Nature Communications* thanks anonymous reviewers for their contributions to the peer review of this work. Peer review reports are available.

Reprints and permission information is available at <http://www.nature.com/reprints>

Publisher's note Springer Nature remains neutral with regard to jurisdictional claims in published maps and institutional affiliations.



Open Access This article is licensed under a Creative Commons Attribution 4.0 International License, which permits use, sharing, adaptation, distribution and reproduction in any medium or format, as long as you give appropriate credit to the original author(s) and the source, provide a link to the Creative Commons license, and indicate if changes were made. The images or other third party material in this article are included in the article's Creative Commons license, unless indicated otherwise in a credit line to the material. If material is not included in the article's Creative Commons license and your intended use is not permitted by statutory regulation or exceeds the permitted use, you will need to obtain permission directly from the copyright holder. To view a copy of this license, visit <http://creativecommons.org/licenses/by/4.0/>.

© The Author(s) 2019

Supplementary Information for

Contribution of oxic methane production to
surface methane emission in lakes and its
global importance

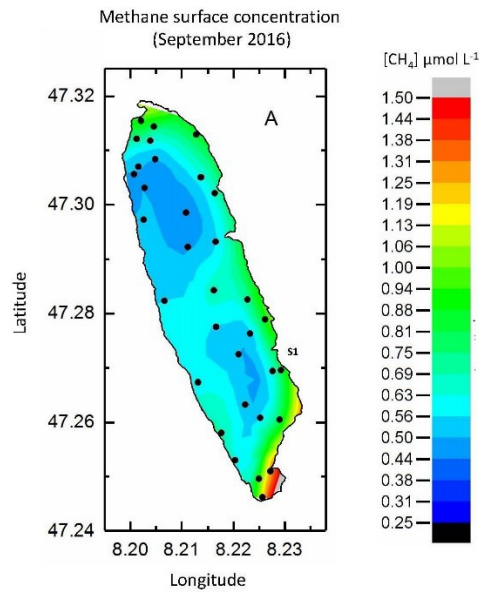
by Günthel et al.

Supplementary Note 1: Re-analysis of Lake Hallwil surface mixed layer (SML) methane mass balance (June-August 2016)

We re-analyzed the Lake Hallwil methane mass balance¹ applying a bathymetry based on the Swiss topographic map of the lake, which was confirmed by a bathymetric survey². The analysis was performed reconsidering the key variables for the methane budget: (a) littoral methane flux contribution and (b) methane evasion to the atmosphere. The other budget components (methane oxidation, input from rivers and diffusion from the hypolimnion) play a minor role in this system and were applied as previously described¹:

Re-calculation of Lake Hallwil bathymetry. The bathymetry of Lake Hallwil used in Donis et al. (2017)¹ is the result of a seismic survey carried out in 2015¹. These measurements lead to the estimation of the lake planar area and sediment area used for the methane mass balance of the surface mixed layer. When estimating these parameters based on a geometric extrapolation from the isolines of the topographic map of Lake Hallwil (<https://www.swisstopo.admin.ch/en/home.html>), the littoral area was underestimated by a factor 7 by Donis et al. (2017)¹. Our map-based calculations give a surface lake area of $9.9 * 10^6 \text{ m}^2$ instead of $8.4 * 10^6 \text{ m}^2$ as previously reported in Donis et al. (2017)¹. The sediment area of the surface mixed layer (5 m deep) is $0.7 * 10^6 \text{ m}^2$ instead of $0.1 * 10^6 \text{ m}^2$, and consequently the surface mixed layer volume equals $48 * 10^6 \text{ m}^3$ instead of $41 * 10^6 \text{ m}^3$.

Lake Hallwil littoral contribution to SML methane budget. As revealed from a survey of surface methane concentration carried out in September 2016, Lake Hallwil's littoral methane production is restricted to some areas of the lake sediments (Supplementary Fig. 1).



Supplementary Figure 1 | Methane surface water concentrations in Lake Hallwil (9th September 2016). Black dots represent the sampling points. S1 indicates the location of measured sediment fluxes - diffusive and ebullitive (see Methods in Donis et al. 2017¹). Source data are provided as a Source Data file.

Sediment methane diffusive fluxes were measured in one of the lake hotspots in September 2016 (S1 in Supplementary Fig. 1 above and Supplementary Fig. 1 in Donis et al. 2017¹). The average diffusive flux value of (mean±SD) $1.75 \pm 0.2 \text{ mmol m}^{-2} \text{ d}^{-1}$ was implemented in the SML budget and assumed to be constant from June to September for the entire littoral sediment area. Similarly, a littoral methane ebullition rate of (mean±SD) $1.2 \pm 0.8 \text{ mmol m}^{-2} \text{ d}^{-1}$, as reported for the same site (S1) by Flury et al. 2010³, was applied to the entire sediment area assuming that bubbles contained 100 % CH₄ that dissolved into the water column and homogeneously distributed in the surface mixed layer.

This conservative approach was adopted to compensate for the uncertainty intrinsic to a system-wide analysis based on discrete measurements. Applying the measured flux obtained from a hot spot to the entire littoral zone provides a conservative estimate of the littoral contribution to the methane concentration in the pelagic surface layer.

Lake Hallwil – surface methane emission. Donis et al.¹ determined the surface methane emission in Lake Hallwil in three ways: (a) in situ measurements with floating chambers, (b) k_{600} -calculations based on wind relationship ($k_{600} = 2 * U_{10}$), (c) k_{600} -calculations using wind relationships from MacIntyre et al. (2010)⁴ for heated water columns (positive buoyancy flux, $k_{600} = 1.74 * U_{10} - 0.15$). We added 3 additional parametrizations: based on wind speed and lake size from Vachon and Prairie (2013)⁵ ($k_{600} = 2.51 + 1.48 * U_{10} + 0.39 * U_{10} * \log_{10}[\text{lake area}]$), and for cooling and mixing water column from MacIntyre et al. (2010)⁴ (negative buoyancy flux, $k_{600} = 2.04 * U_{10} + 2$, and all buoyancy fluxes combined, $k_{600} = 2.25 * U_{10} + 0.16$). We solved for the corresponding flux using Fick's First Law with an average surface CH₄ concentration of 0.3 $\mu\text{mol l}^{-1}$ as reported in Donis et al. (2017)¹. Results are summarized in Supplementary Table 1:

Supplementary Table 1 | Surface methane fluxes in Lake Hallwil.

Type of model	April – August [mmol m ⁻² d ⁻¹]	June – August [mmol m ⁻² d ⁻¹]
Flux chamber	0.6±0.3	0.8±0.1
Hallwil relationship	0.8±0.5	0.8±0.2
MacIntyre et al. (2010)		
- positive buoyancy flux	0.7±0.4	1.0±0.2
- negative buoyancy flux	1.3±0.5	1.6±0.5
- combined buoyancy fluxes	1.0±0.5	1.1±0.6
Vachon and Prairie (2013)	1.4±0.5	1.7±0.2

Listed values as mean±SD

Lake Hallwil SML methane mass balance. Lake Hallwil methane mass balance for the SML was recalculated (equation (3) in Donis et al. 2017¹) with the corrected planar area (A_p), sediment area (A_s) and mixed layer volume (V). In Supplementary Table 2, the lower bound of the mass balance represents the most conservative approach, i.e. using chamber measurements for surface flux (April to August) and littoral sediment flux including CH₄

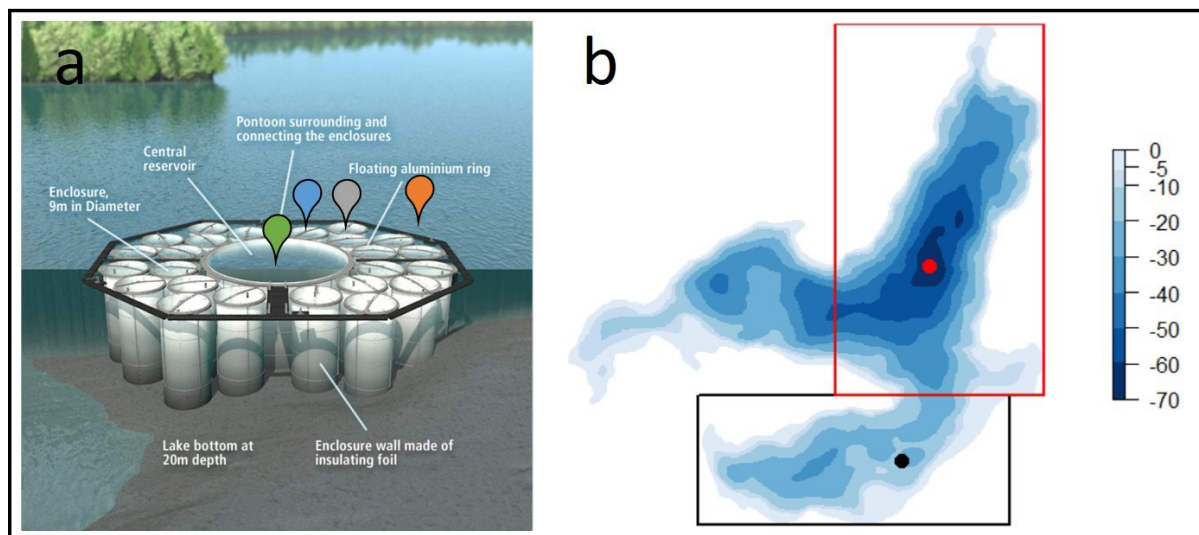
ebullitive input. The upper bound represents the surface fluxes obtained by wind relationship from the study site and reasonably assuming ebullition as a negligible contribution to the pelagic surface methane concentrations.

Supplementary Table 2 | Lower and upper bound values of SML methane mass balance in Lake Hallwil (June – August).

Mass balance component	Symbol	Lower bound [mol d ⁻¹]	Upper bound [mol d ⁻¹]
Surface emission	F_S	5969±2984	7958±1989
Methane oxidation	MO_x	150±8	150±8
Littoral ebullition	$F_{L,eb}$	134±89	0
Littoral diffusion	$F_{L,sed}$	196±22	196±22
River input	F_R	0-207	0-207
Diffusion from thermocline	F_z	252±84	252±84
Internal (oxic) production	$P_{net,s}$	3738±3055	6629±2014
Oxic methane contribution	OMC	63 %	83 %

Note – symbols as in Dohnis et al.¹ Values given as mean±SD

Using these inputs and assumptions, we calculated OMP rates between 78±63 (lower) and 138±42 nmol l⁻¹ d⁻¹ (upper bound); this production rates correspond to a minimum of 63 % and a maximum of 83 % contribution to total emissions from Lake Hallwil to the atmosphere.

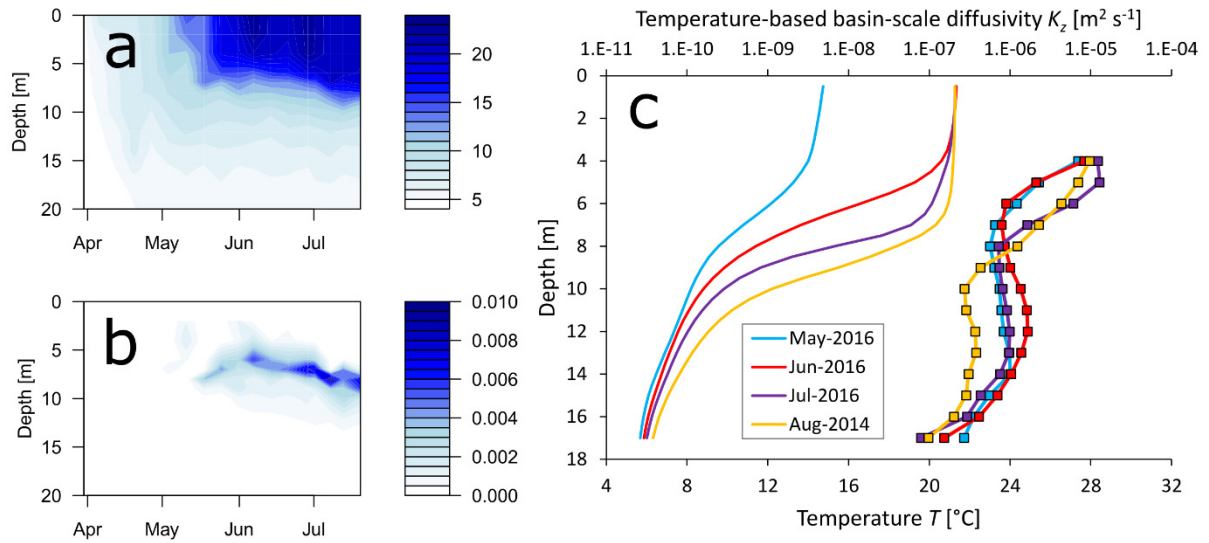


Supplementary Figure 2 | Illustration of the sampling sites and Lake Stechlin's bathymetry. Panel (a), schematics of the lake lab facility (source: <https://www.lake-lab.de/index.php/Design.html>, picture modified) and related sampling locations: central reservoir (green), experimental enclosure 1 (blue), experimental enclosure 13 (grey) and the adjacent open water (orange). Panel (b) depicts the bathymetry of Lake Stechlin [m]. The lake has 3 basins: South (black frame), Northeast (red frame) and North-West basin. Seasonal methane measurements were done at the deepest point (69.5 m deep; red dot) and adjacent to the lake lab facility (20.5 m deep; black dot).

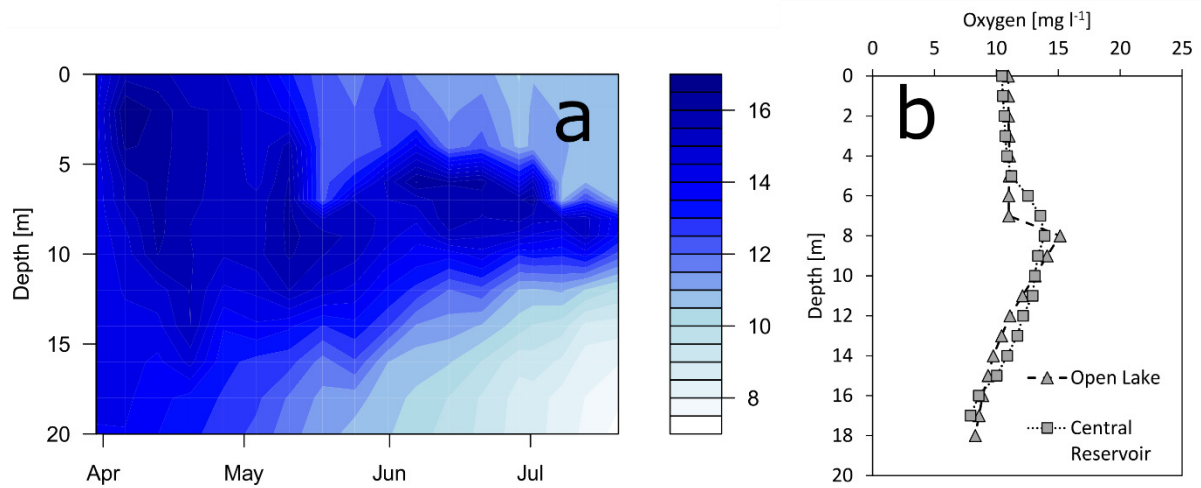
Supplementary Table 3 | Sampling schedule throughout 2014 – 2018. Detailed descriptions on how parameters were recorded can be found in the method section. Measurements in the experimental enclosures were taken 2 weeks after the water had been exchanged with lake water; in contrast, water in the central reservoir has never been exchanged since its installation in 2011/2012. Sampling locations are further described in Supplementary Figure 2.

Year	Month	Location	Purpose	n ^a	WC Profiles ^b	Surface emission ^c	Environmental parameters ^d
2014	Aug	exp. enclosure 1	quantify F_L	4 (SS)	yes	modelled	yes
2014	Aug	exp. enclosure 13	quantify F_L	5 (SS)	yes	modelled	yes
2014	Aug	South basin	quantify F_L	4 (SS)	yes	modelled	yes
2016	Mar-Jul	North basin	seasonal OMP,	6 (SS)	yes	measured (5/6)	yes
			basin variation	13 (NS)	yes	measured (13/13)	yes
2016	Mar-Jul	South basin	seasonal OMP,	6 (SS)	yes	modelled	yes
			basin variation	10 (NS)	yes	modelled	yes
2016	May, Jul	central reservoir	seasonal OMP,	1 (SS)	yes	modelled	yes
			isolated water	2 (NS)	yes	modelled	yes
2018	Jul	North basin	seasonal OMP,	1 (SS)	yes	measured (1/1)	yes
2018	Jul	South basin	seasonal OMP,	1 (SS)	yes	measured (1/1)	yes
			basin variation				

(a) n represents the repetition of methane measurements (each taken on a different day during day time) including water column profile (water samples transferred into glass bottles, crimp-closed, He head space replacement, GC/FID analysis) and surface emission (floating chamber measurements), recordings were taken during the stratified season (SS) or non-stratified/intermediate season (NS); (b) WC profiles indicate water column methane profiles that were taken from the surface down to below the thermocline (ca. 5-7 m depth) in 1 to 2 m increments; (c) surface emission was measured (see methods) using a floating chamber or estimated from a wind based model developed from our own floating chamber measurements and compared to models in the literature (details in Supplementary Note 2); (d) environmental parameters include wind data that were recorded in 10 m above lake surface by the Neuglobsow weather station next to Lake Stechlin and were provided by the Umweltbundesamt, water temperature was recorded by automated YSI probes permanently mounted on the lake lab facility in the South basin (profiling the upper 20 m of the water column continuously in 60 min intervals); F_L is the lateral methane input and OMP is oxidic methane production; in 2016 Lake Stechlin stratified ca. mid-May (see Supplementary Fig. 3a,b); samplings in 2014 and 2018 were done during stratification.



Supplementary Figure 3 | Physical characteristics of the water column. Panel (a): Water column temperature [°C] in 2016 as recorded by a YSI probe. Panel (b): Water column buoyancy frequency N^2 [s⁻¹] in 2016, computed from temperature profiles using the R-package rLakeAnalyzer⁶. Panel (c): Water column temperature (T ; smooth lines) recorded by automated YSI probes measuring continuously in a 30 min and 0.5 m interval and averaged monthly. Basin-scale diffusivity (K_z ; squares) was calculated as after the heat-budget method from temperature data for stratified periods (monthly averages). Source data are provided as a Source Data file.



Supplementary Figure 4 | Oxygen measurements. Panel (a): Water column oxygen concentration [mg l⁻¹] in the open lake (South basin, 2016). Panel (b): Discrete measurements of water column oxygen concentration taken on 7th July 2016 in the open lake and inside the central reservoir. Oxygen was measured using a YSI probe. Source data are provided as a Source Data file.

Supplementary Note 2: Establishing the gas transfer constant (k_{600}) – wind speed (U_{10}) relationship

Using the general gas transfer formula (supplementary equation (S1)), the measured surface methane emission (F_S) and surface water methane (c_{water}), gas transfer constants (k_{CH_4}) were calculated (atmospheric methane content $c_{\text{air}} = 1.88$ ppm) as:

$$k_{\text{CH}_4} = \frac{F_S}{(c_{\text{water}} - c_{\text{air}})}; [\text{cm h}^{-1}] \quad (\text{S1})$$

Subsequently, the k_{CH_4} values were transformed into k_{600} values:

$$k_{600} = \frac{k_{\text{CH}_4}}{\left(\frac{Sc_{\text{CH}_4}}{600}\right)^q}; [\text{cm h}^{-1}] \quad (\text{S2})$$

Where Sc_{CH_4} is the dimensionless Schmidt number (computed after Engle & Maleck⁷) and q is a conversion factor with a value of $(-1/2)$ for wind speeds ≥ 3.7 m s⁻¹ and $(-2/3)$ for wind speeds below (Jähne et al.⁸). The k_{600} values were plotted over wind speed (U_{10}) and the obtained linear relationship was then used to estimate missing methane surface emissions. Supplementary Table 3 illustrates measured and estimated surface emissions and related parameters using the established gas-transfer model. The conversion of methane surface fluxes to k_{600} values and plotting over U_{10} yielded the following relationship: $k_{600} [\text{cm h}^{-1}] = 1.98 * U_{10} [\text{m s}^{-1}] + 0.94$ ($R^2 = 0.44$, $p < 0.01$) (Supplementary Table 4). Surface methane emission rates for the South basin were additionally computed using alternative gas-transfer models from the literature (Supplementary Table 7). Results indicate that our gas transfer model predicts values close to the mean values predicted by the alternative models.

Supplementary Table 4 | Data summary of parameters for estimating methane surface emission based on the k_{600} -wind relationship.

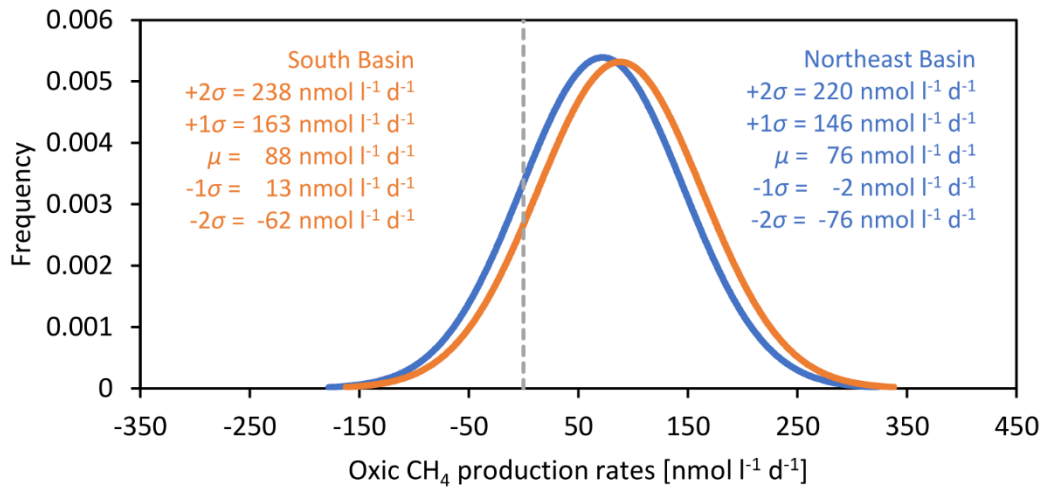
Date	Site	t	U_{10}	T_{SW}	$C_{CH_4 SW}$	L	Sc	$\Delta_{CH_4}^a$	k_{CH_4}	k_{600}	F_5
[dd/mm/yyyy]		[hh:mm]	[m s ⁻¹]	[°C]	[$\mu\text{mol l}^{-1}$]	[mol l ⁻¹ atm ⁻¹]	[]	[$\mu\text{mol l}^{-1}$]	[cm h ⁻¹]	[cm h ⁻¹]	[mmol m ⁻² d ⁻¹]
08/03/2016	NE	14:00	3.9	3.2	0.02221	0.00235	1560.74	0.01779	7.012	11.309	0.030
15/03/2016	NE	14:00	2.3	3.3	0.03132	0.00234	1553.23	0.02691	5.000	9.427	0.032
21/03/2016	NE	12:00	4.7	3.7	0.04525	0.00232	1522.61	0.04089	8.743	13.927	0.086
30/03/2016	NE	10:00	3.1	4.2	0.04487	0.00228	1469.43	0.04059	4.749	8.629	0.046
05/04/2016	NE	13:30	1.3	7.3	0.06804	0.00209	1220.80	0.06410	3.246	5.212	0.050
12/04/2016	NE	12:30	1.4	6.7	0.07852	0.00213	1268.07	0.07452	2.015	3.319	0.036
26/04/2016	NE	12:00	3.1	8.1	0.13658	0.00205	1166.56	0.13272	6.578	10.248	0.210
03/05/2016	NE	13:00	1.9	9.7	0.11743	0.00197	1063.82	0.11373	3.175	4.651	0.087
10/05/2016	NE	12:00	3.8	13.5	0.18101	0.00179	858.09	0.17763	7.707	9.216	0.329
17/05/2016	NE	15:00	n. a.	13.0	0.19187	0.00182	884.33	0.18845	12.363	16.012	0.559
24/05/2016	NE	12:00	3.8	16.9	0.26583	0.00166	717.28	0.26271	5.152	5.633	0.325
31/05/2016	NE	12:00	0.6	19.1	0.35005	0.00159	644.75	0.34707	1.890	1.983	0.157
06/06/2016	NE	13:00	2.0	22.0	0.57289	0.00150	559.39	0.57008	3.545	3.383	0.485
13/06/2016	NE	13:00	1.4	19.5	0.43072	0.00157	632.03	0.42776	2.613	2.705	0.268
20/06/2016	NE	13:00	2.7	20.2	0.70184	0.00155	609.92	0.69892	6.247	6.299	1.048
07/07/2016	NE	14:30	3.4	20.1	0.36378	0.00155	613.14	0.36086	4.660	4.728	0.404
12/07/2016	NE	15:00	4.1	20.8	0.40794	0.00153	592.46	0.40506	3.493	3.471	0.340
19/07/2016	NE	15:00	2.5	20.0	0.38773	0.00156	614.61	0.38480	3.086	3.136	0.285
30/03/2016	S	12:30	3.3	4.7	0.04618	0.00225	1427.42	0.04195	4.855	7.489	0.049
05/04/2016	S	16:00	2.0	7.5	0.07498	0.00209	1212.91	0.07105	3.453	4.910	0.059
12/04/2016	S	15:00	1.2	7.6	0.11609	0.00208	1202.91	0.11218	2.347	3.323	0.063
19/04/2016	S	13:30	9.3	7.9	0.11907	0.00206	1183.86	0.11519	12.327	19.392	0.341
26/04/2016	S	14:30	2.0	8.6	0.13230	0.00203	1135.32	0.12849	3.569	4.910	0.110
03/05/2016	S	15:30	6.4	11.0	0.15123	0.00190	986.56	0.14765	9.790	13.639	0.347
10/05/2016	S	14:30	3.6	14.7	0.28610	0.00174	803.93	0.28282	6.984	8.084	0.474
17/05/2016	S	17:30	0.0	13.6	0.21174	0.00179	854.36	0.20838	0.790	0.942	0.039
24/05/2016	S	14:30	5.0	18.4	0.26537	0.00161	665.19	0.26235	10.140	10.861	0.638
31/05/2016	S	14:30	1.4	20.4	0.39583	0.00155	604.04	0.39293	3.707	3.720	0.350
06/06/2016	S	15:30	2.2	23.0	0.50423	0.00147	534.33	0.50147	5.623	5.307	0.677
13/06/2016	S	15:30	2.0	20.6	0.66523	0.00154	598.11	0.66234	4.918	4.910	0.782
20/06/2016	S	15:30	2.9	20.6	0.63610	0.00154	599.96	0.63320	6.696	6.695	1.018
07/07/2016	S	17:00	4.1	20.1	0.44668	0.00155	611.97	0.44376	8.957	9.076	0.954
12/07/2016	S	17:30	2.6	20.8	0.46059	0.00153	591.90	0.45771	6.142	6.100	0.675
19/07/2016	S	17:30	1.9	20.4	0.46982	0.00155	605.54	0.46691	4.690	4.712	0.526
03/05/2016	CR	16:30	6.7	11.0	0.01316	0.00190	985.72	0.00958	10.152	14.135	0.023
10/05/2016	CR	15:30	3.2	16.3	0.00707	0.00168	740.05	0.00391	6.475	7.191	0.006
07/07/2016	CR	18:00	2.8	20.1	0.01001	0.00155	612.85	0.00709	6.429	6.497	0.011
04-13/08/2014 ^b	S	6-21:00	2.1	23.7	0.58419	0.00145	517.76	0.58146	5.506	5.115	0.768
04-13/08/2014 ^b	E1	6-21:00	2.1	23.7	0.36739	0.00145	517.76	0.58146	5.506	5.115	0.482
04-13/08/2014 ^b	E13	6-21:00	2.1	23.7	0.29207	0.00145	517.76	0.58146	5.506	5.115	0.382

Site – sampling site (Northeast basin – NE: 53°09'20.2"N 13°01'51.5"E / South basin – S: 53°08'35.8"N 13°01'43.2"E / central reservoir – CR: 53°08'35.8"N 13°01'41.1"E / enclosure 1 – E1: 53°08'36.4"N 13°01'41.6"E / enclosure 13 – E13: 53°08'36.5"N 13°01'42.1"E); t – time; U_{10} – wind speed recorded at 10 m above lake surface; T_{SW} – surface water temperature; $C_{CH_4 SW}$ – surface water methane concentration; L – methane solubility; Sc – Schmidt number; Δ_{CH_4} – CH_4 gradient between surface water and air ($= C_{water} - C_{air}$); k – wind dependent gas transfer constants; F_5 – methane water-to-air flux; ^a assuming 1.88 ppm methane content in the atmosphere; ^b corresponding parameters U_{10} , T_{SW} and $C_{CH_4 SW}$ were averaged for day times (06:00 – 21:00, local times) and given dates; n. a. – not available

Supplementary Table 5 | Mass balance components for estimating the lateral methane source. Oxidic production rates computed for the mesocosm enclosures were applied to the mass balance for the open water giving the average lateral methane input.

Site	Mass Balance Component	Symbol	Whole System		Per Volume
			[mol d ⁻¹]	[kg d ⁻¹]	[nmol l ⁻¹ d ⁻¹]
Experimental Enclosures	Surface emission	F_S	(2.7±0.5)E-2	(4.4±0.7)E-4	72.0±11.7
	Methane oxidation	MO_x	1.2E-2	1.9E-4	30.3
	Lateral sediment input	F_L	0	0	0
	Diffusion from thermocline	F_z	(4.3±5.8)E-4	(6.9±9.3)E-6	1.1±1.5
	Internal (oxic) production	P_{net}	(3.9±0.6)E-2	(6.2±1.0)E-4	101.1±16.8
South basin	Surface emission	F_S	862.7	13.8	150.7
	Methane oxidation	MO_x	173.7	2.8	30.3
	Lateral sediment input	F_L	437.1±67.2	7.0±1.1	76.3±11.7
	Diffusion from thermocline	F_z	19.1	0.3	3.3
	Internal (oxic) production	P_{net}	578.9±96.2	9.3±1.5	101.1±16.8

Measurements were taken inside experimental enclosure 1 (20 m deep; 53°08'36.4"N 13°01'41.6"E) and 13 (20 m deep; 53°08'36.5"N 13°01'42.1"E), as well as in the open water adjacent to the enclosures (20.5 m deep; 53°08'36.6"N 13°01'42.8"E) in the South basin of Lake Stechlin. Measurements were taken 4-5 times inside the enclosures and 4 times in the open lake on different days during the period 4-13th August 2014. Methane profiles and surface fluxes were averaged for the mass balance. Surface area: enclosures each 63.6 m², South basin 1,122,775 m². Monte Carlo simulation (9999 iterations) was used to solve the mass balance after the target component (in bold). Values listed are mean±SD.



Supplementary Figure 5 | Density curve of oxic methane production rates obtained from mass balance. Monte Carlo simulation was conducted to solve methane mass balance (9999 iterations). The density function was computed as $f(x) = (1/\sqrt{2\pi}\sigma)e^{-((x-\mu)^2/(2\sigma^2))}$. σ is the standard deviation and μ is the mean value. Source data are provided as a Source Data file.

Supplementary Note 3: Estimating the oxic methane contribution (*OMC*) for additional lakes

As shown by DelSontro et al.'s⁹ model for lateral transport alongside transects and actual transect measurements, methane concentrations of transect measurements reach a plateau phase at distances (corresponds to equivalent radius) ≥ 2 km (equivalent to lake surface areas > 12.6 km²). Vertical diffusion from lower water layers into the surface mixed layer (SML) is a minor methane source, and lateral input and (oxic) internal production are the major sources of SML methane. Therefore, plateau concentrations in transect measurements represent the result of internal production while concentrations above plateau concentration represent the result of lateral transport. To estimate the dimension of both major methane sources, first the plateau concentration was integrated over the lakes' equivalent radius (resembling a measure of the oxic methane source), then elevated methane concentration were integrated over the distance of the gradient (resembling a measure of anoxic/lateral methane source) and finally the *OMC* ratio was calculated as oxic measure divided by the sum of oxic and anoxic measure. Supplementary Table 6 shows *OMC* estimations for lakes with equivalent radii above 2 km.

Supplementary Table 6 | Estimations of oxidic methane contribution for lakes with equivalent radii > 2 km. Transect data were extracted from the DelSontro et al.⁹ study. A graphical approach was used to compute estimates of the lateral and oxidic methane sources.

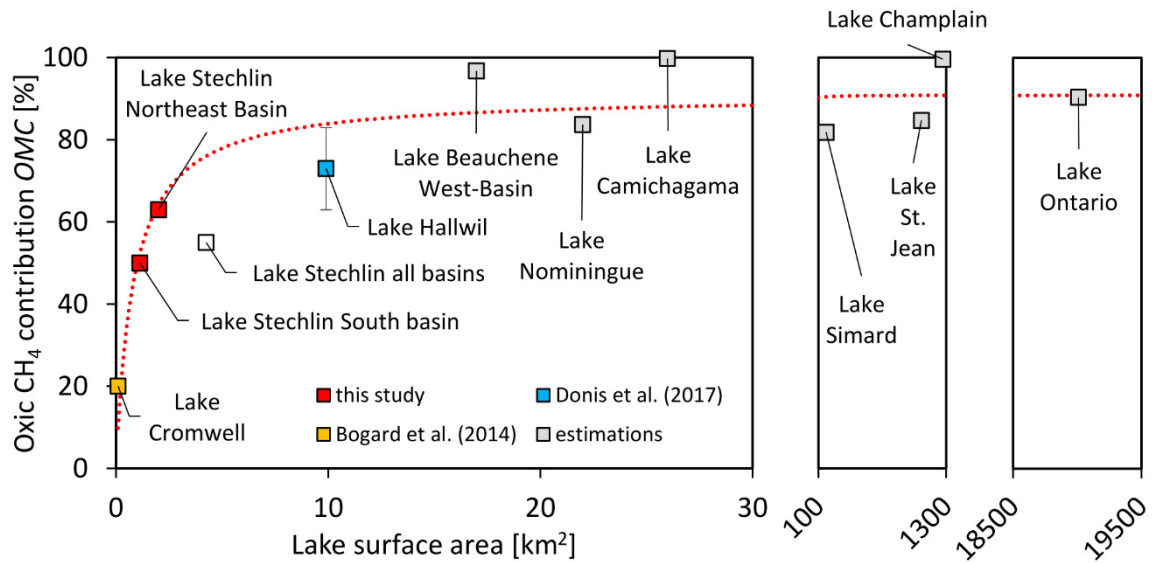
Lake name	Location [coordinate North, West]	A_{tot} [km ²]	R [km]	z_{SML} [m]	A_{sed} [m ²]	V [m ³]	OMC [%]	TP [μg l ⁻¹]
Beauchene (West basin)	46°39'22.7"N, 78°56'53.2"W	17	2.3	5	1.0E+05	8.5E+07	97	3.5
Champlain	44°29'07.4"N, 73°19'08.8"W	1269	20.1	10	1.3E+07	1.3E+10	100	15.2
Camichagama	47°49'54.1"N, 76°19'01.9"W	26	2.9	7	1.8E+05	1.8E+08	100	7.1
Nominingue	46°25'58.1"N, 74°59'33.0"W	22	2.7	5	1.2E+05	1.1E+08	84	8.5
Ontario	43°37'51.6"N, 77°11'06.4"W	19009	77.8	12	2.0E+07	2.3E+11	90	3.7
Simard	47°37'37.9"N, 78°43'02.3"W	170	7.3	10	6.5E+05	1.7E+09	82	21.4
St. Jean	48°31'43.0"N, 71°54'27.4"W	1065	18.4	5	8.2E+05	5.3E+09	85	9.8

A_{tot} – lake surface area, R – equivalent radius, z_{SML} – depth of the surface mixed layer, V – volume of the surface mixed layer, OMC – oxidic methane contribution, TP – total phosphorus level indicating the trophic state: oligo- (0 – 12 μg l⁻¹), meso- (12 – 24 μg l⁻¹) or eutrophic (>24 μg l⁻¹). Calculation of equivalent radius assumes circular shape of lake surface. OMC calculation assumes a maximum lateral methane transport up to 2 km.

Equivalent radius (R). The equivalent radius was calculated to make lakes with different morphology comparable, by assuming the lakes' surface area (A_{tot}) to be of circular shape and solving $A_{tot} = \pi R^2$ for R . Values for A_{tot} were derived from DelSontro et al.⁹.

Volume of the surface mixed layer estimation (V). The volume of the surface mixed layer was calculated by multiplying lake surface area (A_{tot}) with depth of the surface mixed layer (z_{SML}). Both parameters were retrieved from Supplementary Information of DelSontro et al.⁹.

Sediment area estimation (A_{sed}). The sediment area was estimated by computing the perimeter of the lake from lake surface area (A_{tot}) assuming circular lake shape. The perimeter was then multiplied by the average distance (d) littoral sediments reach into the surface mixed layer and into depth (z_{SML}). Assuming the sediments decline at a 45°-degree angle towards lake center, d was computed based on the depth of the surface mixed layer (z_{SML}) and Pythagorean theorem. Morphological lake parameters needed for these transformations were derived from DelSontro et al.⁹.

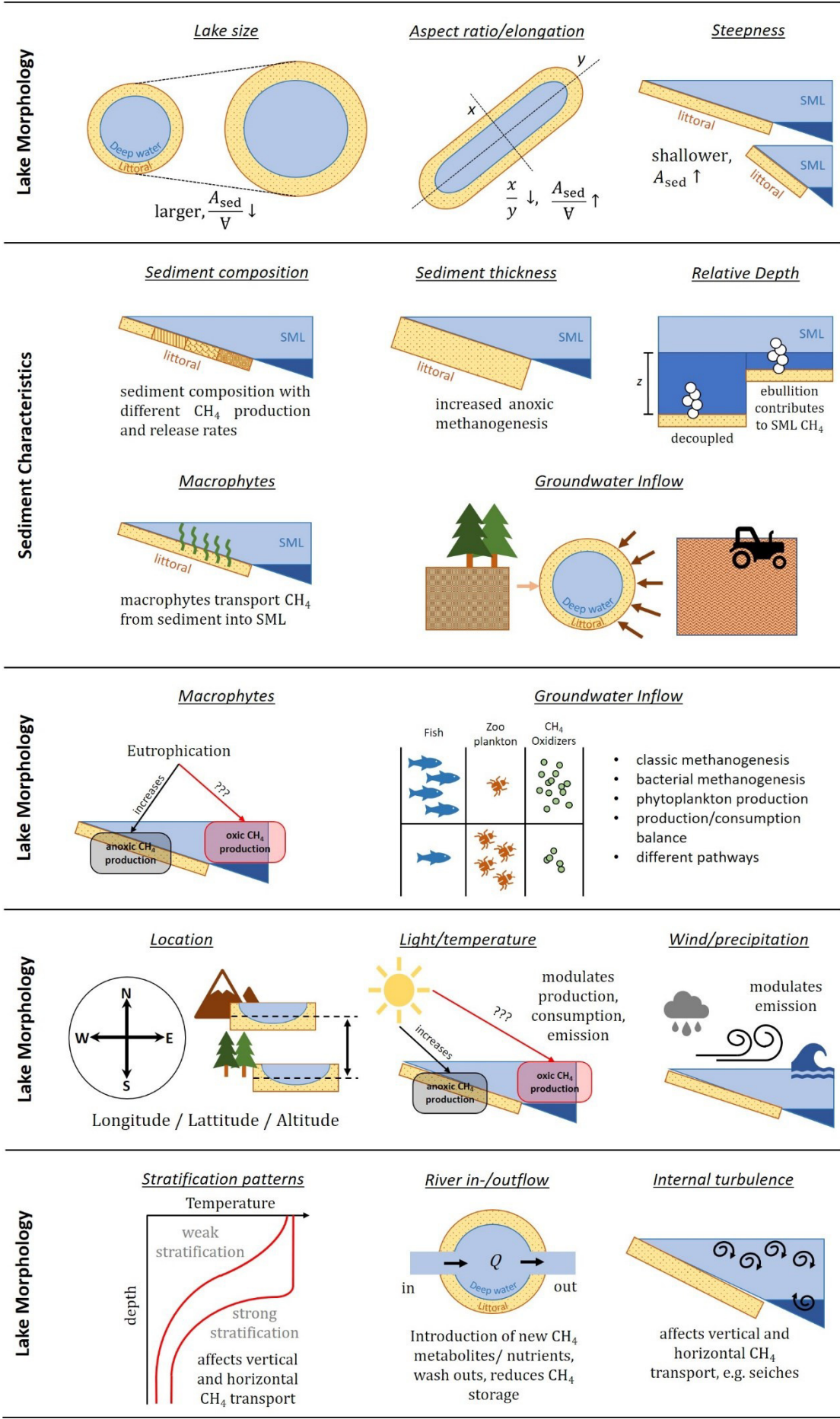


Supplementary Figure 6 | Oxidic methane contribution in relation to lake size. Mass balance results, together with literature data and estimates (see Supplementary Note 3), follow a function of the type $y = (a * x)/(b + x)$. Deploying least standard error (*SE*) method gave the minimum standard error of 8.6 % when $a = 90.87$ and $b = 0.83$ (red line); indicating that the oxidic source is the major SML methane source in lakes sized larger than 1 km². The value for Lake Hallwil was updated as described in Supplementary Note 1; the upper and lower bound estimates are represented by error bars and the mean was used to establish the trend line function. The *x*- and *y*-axes are linearly scaled. In an alternative analysis where the datasets for Lake Stechlin’s two basins were combined (open square symbol), the equation constants change slightly ($a = 92.90$, $b = 1.92$, $SE = 10.7$ %). In this case the empirical model predicts the oxidic methane source to be the dominant source in lakes larger than 2 km². Standard error *SE* was computed as $SE = \sqrt{\sum(\hat{x} - x)^2/(n - 2)}$ where \hat{x} is the predicted value, *x* is the data point value and *n* is the number of data points. Supplementary Table 3 gives details on sampling schedules for Lake Stechlin. Source data are provided as a Source Data file.

Supplementary Table 7 | Summary of surface emission and mass balance results for Lake Stechlin's South basin using June-July 2016/2018 data and different gas transfer models.

Type of model	F_S [mmol m ⁻² d ⁻¹]	P_{net} [nmol l ⁻¹ d ⁻¹]	OMC [%]
Stechlin relationship	0.772±0.186	109±61	55
Hallwil relationship	0.657±0.181	73±60	45
MacIntyre et al. (2010)			
- positive buoyancy flux	0.552±0.156	41±52	32
- negative buoyancy flux	0.925±0.201	155±64	64
- combined buoyancy fluxes	0.759±0.204	104±66	54
Vachon and Prairie (2013)			
- based on wind	1.027±0.243	185±77	68
- based on wind, lake area	0.813±0.160	120±53	58

F_S – surface methane emission; P_{net} – internal (oxic) methane production; OMC – contribution of internal (oxic) methane production to the system-wide surface emission. Stechlin relationship was developed based on flux chamber measurements: $k_{600} = 1.98 * U_{10} + 0.94$ (k_{600} – gas transfer constant [cm h⁻¹]; U_{10} – wind speed at 10 m height [m s⁻¹]). Donis et al. (2017)¹/Supplementary Note 1 - Hallwil relationship: $k_{600} = 2 * U_{10}$. MacIntyre et al. (2010)⁴ relationships: $k_{600} = 1.74 * U_{10} - 0.15$ (at buoyancy flux $\beta > 0$); $k_{600} = 2.04 * U_{10} + 2.0$ ($\beta < 0$); $k_{600} = 2.25 * U_{10} + 0.16$ (all β). Vachon and Prairie (2013)⁵ relationships: $k_{600} = 2.58 * U_{10} + 1.41$; $k_{600} = 1.48 * U_{10} + 0.39 * U_{10} * \log_{10}(LA) + 2.51$ where LA is lake area [km²] (here we used basin area instead of whole-lake area). Listed values as mean±SD of 6 replicates (2016 data).



Supplementary Figure 7 / Examples of factors affecting the contribution of oxic and anoxic methane sources to the system-wide surface emission. Factors are categorized into lake morphology, sediment characteristics, nutrient conditions/ecology, meteorology and lake physics. A_{sed} symbolizes littoral sediment area, SML is surface mixed layer, V refers to the volume of the surface mixed layer and Q is flow rate.

Supplementary Note 4: First-order estimation of oxidic methane contribution (*OMC*) in a global context

We used the established model of *OMC* in relation with lake surface area (Supplementary Fig. 5) to get a first-order estimate of how much oxidic methane production potentially contributes to the surface methane emission of lakes on a global scale. Our model is based data from temperate lakes with oligo to mesotrophic nutrient state. It is not meant to represent the biological, physical and geological complexity of all lakes; rather, it is used as a predictive tool to assess the potential global relevance of *OMP* based on simple lake morphology.

Global lake size class data for lakes $\geq 0.01 \text{ km}^2$ were extracted from Cael et al.¹⁰: this includes the abundance (n) and their total surface area (A_{class} ; [km^2]). The percentage contribution of each lake size class to the global surface area (γ_{class} ; [%]) was computed where global lake surface area (A_{global}) is 5,128,000 km^2 :

$$\gamma_{\text{class}} = \frac{A_{\text{class}} * 100 \%}{A_{\text{global}}}; [\%] \quad (\text{S3})$$

The mean size of the lake size class (A_{mean} ; [km^2]), which is the average of the upper and lower limits of the size class, was applied to the *OMC*-lake size empirical model (Supplementary Fig. 6) to compute the *OMC* value for each lake size class (OMC_{class} ; [%]):

$$OMC_{\text{class}} = \frac{90.87 * A_{\text{mean}}}{0.83 + A_{\text{mean}}}; [\%] \quad (\text{S4})$$

The *OMC* values for the different lake size classes (OMC_{class}) was subsequently projected to the global lake inventory relative to the total surface area (γ_{global} ; [%]) by multiplying OMC_{class} values by γ_{class} :

$$\gamma_{\text{global}} = \frac{\gamma_{\text{class}}}{100\%} * OMC_{\text{class}}; [\%] \quad (S5)$$

The OMC estimate for the global lake inventory (OMC_{global} ; [%]) was finally computed by summing up the γ_{global} of all lake size classes:

$$OMC_{\text{global}} = \sum \gamma_{\text{global}}; [\%] \quad (S6)$$

By accounting for the different *OMC* values of the lake size classes and the different contributions of these lake size classes to the global lake surface area, the first-order estimate for the global *OMC* was calculated to be 66 %. Supplementary Table 8 summarizes the parameters calculated for this estimation. For future applications, the model can be improved with data from different lake types, such as eutrophic lakes and lakes in other climate zones, which might deviate from the present predictive function, especially for smaller lakes.

Supplementary Table 8 | First-order estimate of the global relevance of oxidic methane contribution to the surface methane emission in lakes (*OMC*). The global abundance of different lake size classes and the total surface area was extracted from Cael et al.¹⁰ The mean lake size was applied to the established *OMC*~lake surface area model to compute *OMC* estimations for different lake size classes. These *OMC* values were then projected to the total surface area of the lake size classes.

Literature values		Applying model				Projection to global total surface area
Lake size class [m ²]	Abundance <i>n</i> [#]	Total surface area <i>A</i> _{class} [km ²]	Total surface area γ _{class} [%]	Lake size mean <i>A</i> _{mean} [km ²]	Lake size class <i>OMC</i> _{class} [%]	Global <i>OMC</i> per size class γ _{global} [%]
10 ⁴ – 10 ⁵	23725071	683000	13.32	0.05	5.17	0.69
10 ⁵ – 10 ⁶	3813612	995000	19.40	0.5	34.21	6.64
10 ⁶ – 10 ⁷	331452	793000	15.46	5	77.96	12.06
10 ⁷ – 10 ⁸	24332	611000	11.91	50	89.39	10.65
10 ⁸ – 10 ⁹	1948	489000	9.54	500	90.72	8.65
10 ⁹ – 10 ¹⁰	211	537000	10.47	5000	90.85	9.51
>10 ¹⁰	20	1020000	19.89	50000	90.86	18.07
Σ Global	27896646	5128000				66.27

Supplementary Table 9 | Mass Balance parametrization for the stratified and non-stratified periods.

Component	Terminus	Symbol	Open Lake		Lake Lab Enclosures/Mesocosms (stratified condition)	
			Stratified condition	Unstratified condition	Enclosure E1 & E13	Central Enclosure
Changing CH ₄ accumulation	$\frac{\partial C}{\partial t} * \forall$		= 0 (steady state)	= 0 (steady state)	= 0 (steady state)	= 0 (steady state)
CH ₄ river input	$(Q_R * C_R)$		= 0	= 0	= 0	= 0
Vertical CH ₄ diffusion from metalimnion	$(A_{th} * F_z)$	$A_{th}^a(NE)$ $A_{th}^a(S)$ F_z	= 1,757,475 / 1,725,100 / 1,694,600 m ² = 832,600 / 808,000 / 78,150 m ² = $K_z * C'$	= 0 = 0 = $K_z * C'$	= 63.6 m ² = $K_z * C'$	= 706.9 m ² = $K_z * C'$
CH ₄ sediment flux	$(A_{sed} * F_L)$	$A_{sed}^a(NE)$ $A_{sed}^a(S)$ F_L	= 249,225 / 281,600 / 312,100 m ² = 290,175 / 314,775 / 335,625 m ² = 1.4±0.2 mmol m ⁻² d ⁻¹	= 2,006,700 m ² = 1,122,775 m ² = 0 mmol m ⁻² d ⁻¹	= 0 mmol m ⁻² d ⁻¹ = 0 mmol m ⁻² d ⁻¹	= 0 mmol m ⁻² d ⁻¹ = 0 mmol m ⁻² d ⁻¹
CH ₄ oxidation rate	$(MOx * \forall)$	MOx $\forall^a(NE)$ $\forall^a(S)$	= 0 * P_{net} = 9,439,750 / 11,197,225 / 12,922,325 m ³ = 4,893,575 / 5,726,175 / 6,534,175 m ³	= 0.3 * P_{net} = 59,843,550 m ³ = 16,857,425 m ³	= 0.3 * P_{net} = 318.1 / 381.7 / 445.3 m ³	= 0.3 * P_{net} = 3534.3 / 4241.2 / 4948.0 m ³
Water-to-air CH ₄ flux	$(A_{tot} * F_S)$	A_{tot} F_S^b	= 4,249,625 m ² = measured (NE) / computed (S)	= 4,249,625 m ² = measured (NE) / (S) computed	= 63.6 m ² = computed	= 706.9 m ² = computed
Internal CH ₄ production rate	$(P_{net} * \forall)$	P_{net} $\forall^a(NE)$ $\forall^a(S)$	= target parameter; = 9,439,750 / 11,197,225 / 12,922,325 m ³ = 4,893,575 / 5,726,175 / 6,534,175 m ³	= target parameter = 59,843,550 m ³ = 16,857,425 m ³	= target parameter = 318.1 / 381.7 / 445.3 m ³	= target parameter = 3534.3 / 4241.2 / 4948.0 m ³

\forall - volume of the mixed layer [m³]; C – methane concentration in the water column [mol m⁻³]; t – time [d]; Q_R – inflow rate of river water [m³ s⁻¹]; C_R – methane concentration in river water [mol m⁻³]; A_{th} – planar area of thermocline [m²]; A_{sed} – sediment area of the mixed layer; A_{tot} – total surface area of the lake [m²]; F_z – internal turbulent diffusion from metalimnion to the surface mixed layer [mol m⁻² d⁻¹]; F_L – laterally transported methane [mol m⁻² d⁻¹]; F_S – water-to-air methane flux [mol m⁻² d⁻¹]; MOx – methane oxidation rate [mol m⁻³ d⁻¹]; P_{net} – internal methane production [mol m⁻³ d⁻¹]; ^a depending on seasonal stage the mixed layer was either 5 (May/ June), 6 (July) or 7 m deep (August) leading to different dimensions of A_{th} , A_{sed} and \forall while the whole water column was assumed to be mixed during the unstratified season; ^b methane emission at the surface was either measured using a combination of floating chamber and GC/FID unit (Northeast basin dataset; **NE**) or computed (South basin dataset; **S**) as after the linear relationship between gas transfer constants (k) and wind speed (U_{10}): $k \sim U_{10}$.

0

1 **Supplementary Note 5: Vertical turbulent diffusivities (K_z) in the**
2 **open lake and enclosures**

3 The open-water column temperature adjacent to the mesocosm enclosures was
4 recorded by an auto-profiler (30 min interval; between 0.5 and 20 m depth in 0.5 m
5 increments) for the entire study period. The coefficient of the effective turbulent exchange
6 K_{zT} was estimated from temperature T within the water column of depth $H = 20$ m using the
7 flux-gradient method^{11,12}:

8
$$K_{zT}(z) = -\frac{\int_H^z \frac{\partial T}{\partial t}}{\left(\frac{\partial T}{\partial z}\right)_z}; [\text{m}^2 \text{s}^{-1}] \quad (\text{S7})$$

9 Additionally, we compared vertical diffusivities in the enclosures and in the open lake
10 using measurements by a free-falling shear microstructure (MSS) profiler MSS-60 (ISW
11 Wassermesstechnik) equipped with two airfoil velocity shear sensors for estimation of
12 dissipation rate of the turbulence kinetic energy (TKE) ε , and a fast response thermistor for
13 estimation of temperature and density fields (Prandke 2005¹³). The instrument was allowed
14 to fall through the water column at a speed of 0.5 m s^{-1} taking measurements at 1024 Hz. To
15 compare the vertical diffusivities inside the mesocosm enclosures and the open lake, 12
16 profiles were taken in one mesocosm enclosures and another 12 profiles in the open lake on
17 3-4 Sep 2013 during daytime at an interval of 30 min to avoid previous mixing produced by
18 the profiler itself. The TKE dissipation rate ε was then calculated from the measured velocity
19 shearing $\partial U/\partial z$ as described by Hinze (1959)¹⁴:

20
$$\varepsilon = \frac{15}{2} \nu \left(\frac{\partial U}{\partial z}\right)^2; [\text{m}^2 \text{s}^{-3}] \quad (\text{S8})$$

21 where $\nu \approx 10^{-6} \text{ m}^2 \text{ s}^{-1}$ is the kinematic viscosity of water.

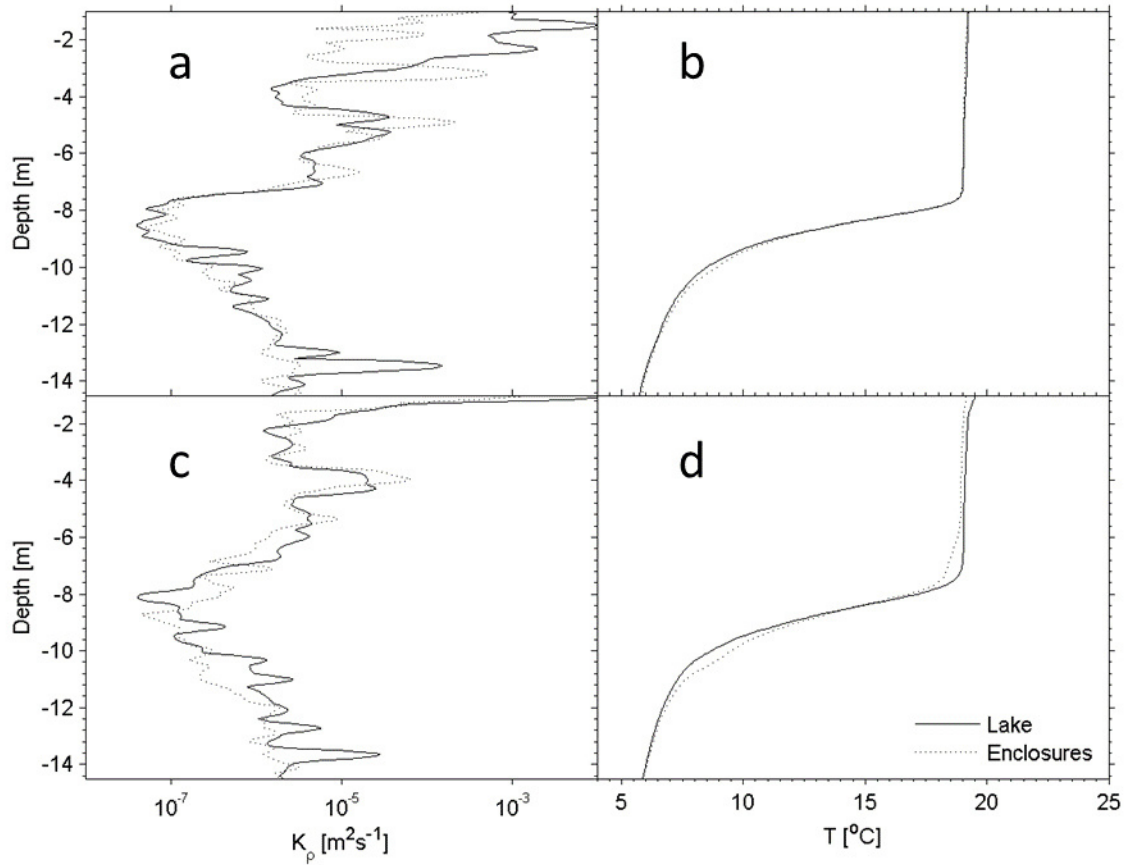
22

23 The mean profiles of the TKE dissipation rate were constructed by averaging over
24 profile series in the open lake and in the enclosures and subsequently averaging over 0.25 m
25 depth intervals. The values of ε were used to estimate the coefficient of vertical density
26 exchange K_ρ according to Kirillin et al. (2012)¹⁵:

$$27 \quad K_\rho = \begin{cases} C_1 \varepsilon^{1/3} z^{4/3} & \text{at } \varepsilon^{1/2} N^{-3/2} \geq \kappa z & \text{at the surface} \\ C_2 \varepsilon N^{-2} & \text{at } \varepsilon^{1/2} N^{-3/2} < \kappa z & \text{in the thermocline} \end{cases} \quad (S9)$$

28 where N is the buoyancy frequency in the thermocline, $C_1 = 0.4^{4/3}$ and $C_2 = 0.2$ (Osborn
29 1980¹⁶). Temperature and diffusivity profiles measured inside the mesocosms were very
30 similar to the open-water profiles for the same period, except the upper several meters of
31 the epilimnion, where wind mixing produced a stronger turbulence in the open lake
32 (Supplementary Fig. 8). This allowed us to apply the same heat-budget estimates of open-
33 water diffusivity values at depths >4 m to estimate the vertical flux in both open lake and
34 mesocosm enclosures for the entire study period.

35



36
37

38 **Supplementary Figure 8 | Physical parameters inside enclosures and in the open lake.**

39 Vertical turbulent diffusion coefficient (**a, c**) and vertical temperature distribution from the
 40 MSS profiling (**b, d**) in the mesocosm enclosures (dotted lines) and in the open lake (solid
 41 lines) under windy condition (Panels **a-b**, 3 Sep 2013, wind speeds 3-5 m s⁻¹) and calm
 42 condition (Panels **c-d**, 4 Sep 2013). Source data are provided as a Source Data file.

43

44 **Supplementary References**

- 45 1. Donis, D. et al. Full-scale evaluation of methane production under oxic conditions in a
46 mesotrophic lake. *Nat. Commun.* **8**, 1661 (2017).
- 47 2. Bierlein, K. A. et al. Increased sediment oxygen flux in lakes and reservoirs: the impact
48 of hypolimnetic oxygenation. *Water Resour. Res.* **53**, 4876-4890 (2017).
- 49 3. Flury, S., et al. Methane emissions from a freshwater marsh in response to
50 experimentally simulated global warming and nitrogen enrichment. *J. Geophys. Res.*
51 **115**, G01007 (2010).
- 52 4. MacIntyre, S. et al. Buoyancy flux, turbulence, and the gas transfer coefficient in a
53 stratified lake. *Geophys. Res. Lett.* **37**, L24604 (2010).
- 54 5. Vachon, D. & Prairie, Y. T. The ecosystem size and shape dependence of gas transfer
55 velocity versus wind speed relationships in lakes. *Can. J. Fish. Aquat. Sci.* **70**, 1757-
56 1764 (2013).
- 57 6. Winslow, L. et al. rLakeAnalyzer: Lake Physics Tools. R package version 1.11.4 at
58 <https://CRAN.R-project.org/package=rLakeAnalyzer> (2018).
- 59 7. Engle, D. & M. Melack, J. Methane emissions from an Amazon floodplain lake:
60 enhanced release during episodic mixing and during falling water. *Biogeochemistry* **51**,
61 71–90 (2000).
- 62 8. Jähne, B. J. et al. On the parameters influencing air-water gas exchange. *J. Geophys.*
63 *Res.* **92**, 1937–1949 (1987).
- 64 9. DelSontro, T., del Giorgio, P. A. & Prairie, Y. T. No longer a paradox: the interaction
65 between physical transport and biological processes explains the spatial distribution
66 of surface water methane within and across lakes. *Ecosystems* **21**, 1073-1087 (2018).

- 67 10. Cael, B. B., Heathcote, A. J. & Seekell, D. A. The volume and mean depth of Earth's
68 lakes. *Geophys. Res. Lett.* **44**, 209–218 (2017).
- 69 11. Powell, T. & Jassby, A. The estimation of vertical eddy diffusivities below the
70 thermocline in lakes. *Water Resour. Res.* **10**, 191-198 (1974).
- 71 12. Dubovskaya, O. P. et al. Effects of water column processes on the use of sediment
72 traps to measure zooplankton non-predatory mortality: a mathematical and empirical
73 assessment. *J. Plankton Res.* **40**, 91-106 (2017).
- 74 13. Prandke, H. in *Marine Turbulence: Theories, Observations, and Models* (eds Baumert,
75 H., Simpson, J. & Sündermann, J.) 101-109 (Cambridge Univ. Press, Cambridge, 2005).
- 76 14. Hinze, J. O. *Turbulence* (McGraw-Hill, New York, 1959).
- 77 15. Kirillin, G., Grossart, H.-P. & Tang, K. W. Modeling sinking rate of zooplankton
78 carcasses: effects of stratification and mixing. *Limnol. Oceanogr.* **57**, 881-894 (2012).
- 79 16. Osborn, T. R. Estimates of the local rate of vertical diffusion from dissipation
80 measurements. *J. Phys. Oceanogr.* **10**, 83–89 (1980).